ELSEVIER

Journal of South American Earth Sciences 24 (2007) 1–24

Journal of
South American
Earth Sciences

www.elsevier.com/locate/jsames

Tectonic evolution and paleogeography of the Mesozoic Pucará Basin, central Peru

Silvia Rosas [a,*], Lluís Fontboté [b], Anthony Tankard [c]

[a] *Pontificia Universidad Católica del Perú, Av. Universitaria s/n, San Miguel, Lima, Peru*
[b] *Section des Sciences de la Terre, rue des Maraîchers, 13, CH-1205 Genève, Switzerland*
[c] *Tankard Enterprises, 71 Lake Crimson Close S.E., Calgary, Alta., Canada T2J 3K8*

Received 1 October 2004; accepted 2 October 2006

Abstract

The Pucará Basin of Peru is an elongate trough that subsided landward of a NNW-trending structural high during the Late Triassic–Early Jurassic. It formed as a postrift regional sag as the earlier Triassic fault-controlled Mitu rifts yoked together. The rift and transitional postrift basins were associated with a NW-striking sinistral shear zone that controlled isopachs and facies distributions and resulted in magmatism and mineralization along its trend. A distinct association of later dolomitization and MVT lead–zinc mineralization also occurs with these basin-forming shear zones. Although basaltic and andesitic extrusives are common, there is no evidence that the Pacific margin was a magmatic arc until the upper Pucará, and then only weakly developed in northern Peru. Except in the upper Pucará of northwest Peru, geochemical studies, including whole rock and trace element analyses, indicate that intercalations of volcanic material have intraplate rift affinities. The basin fill has a three-part stratigraphic subdivision, comprising lower and upper carbonate platforms with an intermediate phase of basin overdeepening and sediment starvation that resulted in a regional, organic-rich argillaceous drape. Stratigraphic accumulation was dominated by axial patterns of onlap and progradation, though facies characteristics show it was augmented by periodic flooding of the western basin margin high. Marine invertebrate fossils indicate normal marine salinities. The sedimentological interpretation is based on a SW–NE transect in the southern part of the Pucará Basin. The Chambará (Norian–Rhaetian) and Condorsinga (Toarcian) formations were constructed principally by shallow-water carbonate sedimentation in lagoon-like subtidal, intertidal, and supratidal paleoenvironments. The subtidal carbonate platform is dominated by oolitic grainstones with subordinate bioclastic packstones. Subordinate open-basin facies in the Chambará Formation consist principally of crinoidal packstones and bioclastic wackestones. In the intertidal and supratidal facies, evaporite pseudomorphs are common and generally associated with algal mats and widespread early diagenetic dolomitization. During the Chambará and Condorsinga, subsidence typically was balanced by carbonate production and shallow-water environments prevailed; the basin had the characteristics of an overfilled basin. Conversely, the intermediate late Rhaetian–Sinemurian stage of basin subsidence was marked by underfilled deep water conditions. This widespread transgressive inundation of the Pucará Basin, recorded in the argillaceous Aramachay stratigraphy, correlates with similar events in other Andean basins.

Keywords: Triassic; Jurassic; Pucara Group; Central Peru; Paleogeography; Tectonic evolution; Sedimentary facies

1. Introduction

The sedimentary basins of Peru record a long history of Phanerozoic subsidence by intermittent reactivation of older fabrics in the continental lithosphere (Tankard et al., 2006). The principal basin-forming faults are conspicuous and, especially in the eastern sections, well documented by an enormous amount of seismic exploration. The structural architecture distinguishes a tract of basins bounded by families of NW- and NE-trending faults; the former have marked strike-slip affinities. For much of their history, these depocenters were unique but at some points

* Corresponding author.
E-mail address: brosas@pucp.edu.pe (S. Rosas).

0895-9811/$ - see front matter © 2007 Elsevier Ltd. All rights reserved.
doi:10.1016/j.jsames.2007.03.002

locally joined together, depending on prevailing stress fields. This history of basin subsidence and intermittent deformation is preserved in a sedimentary cover of terrigenous clastic sediments and subordinate carbonates arranged in a stacked system of unconformity-bounded sequences.

The Pucará Basin of central and northern Peru is the Late Triassic–Early Jurassic stage of basin formation (Fig. 1), characterized by the yoking together of the earlier Mitu rifts as fault-controlled subsidence was superseded by postrift regional subsidence and marine inundation during the Jurassic. This basin complex currently is caught up in the NNW-striking Andean ranges as a welt of structural inversion and transpressional uplift. Locally, this transpression has resulted in shortcut faults with low-angle detachment over short distances (e.g., Tarma; Baudoux et al., 2001). Pronounced thin-skinned structural telescoping characterizes the Ene–Madre de Dios mountain belt of southern Peru. Voluminous literature addresses various aspects of the Pucará Group, including Mégard (1978), Loughman and Hallam (1982), Rosas (1994), Rosas and Fontboté (1995), and Moritz et al. (1996). Several paleontological studies interpret ages and paleogeographies (see Prinz, 1985a,b; Stanley, 1994). We draw on these previous works.

We investigate the sedimentology and tectonic implications of the southern part of the Pucará Basin using a detailed study of six measured sections that span the width of the Pucará depocentre and form a NE-oriented transect. These sections include Tingocancha in a small valley incised into the northeastern part of the Yauli dome; Malpaso and Tarmatambo near the town of Tarma; the San Vicente Mine and Vilcapoma, 2 km NE of the San Vicente mine location; and Shalipayco, which is located nearly 60 km NW of this general transect but shares the same fault zone as San Vicente (Figs. 1b and 6; coordinates for each measured section are documented in Rosas, 1994). The structural framework and tectonic interpretation are derived from a large exploration study (Tankard, 2001). The integration of our results with the data of other authors extends understanding of the sedimentary and tectonic evolution of the Pucará Group. We reveal that the mainly shallow-water carbonate platform deposits accumulated in several depocenters formed by early Mesozoic sub-

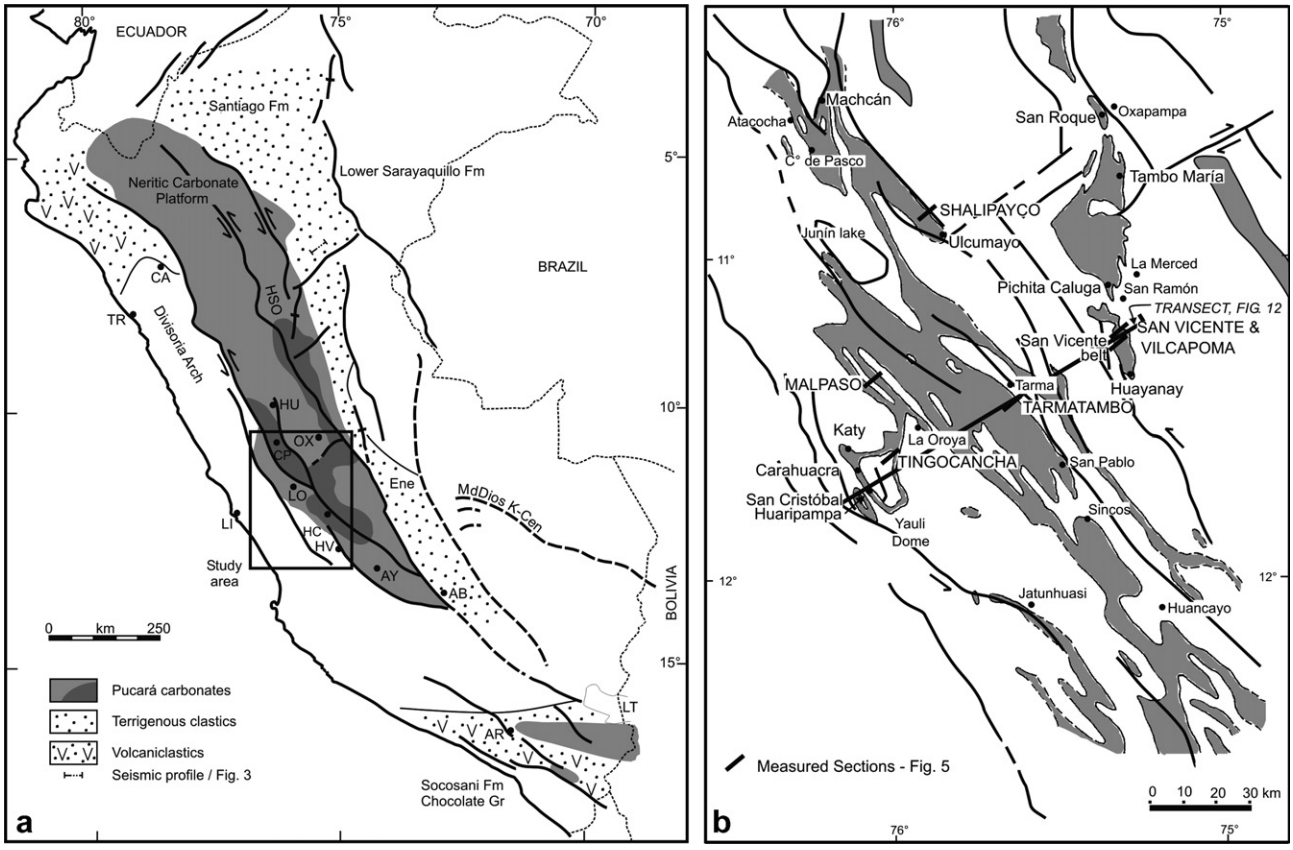

Fig. 1. Distribution of Upper Triassic–Lower Jurassic Pucará cover in Peru. (a) Pucará Basin is separated from the plate margin by a basement high. Pucará distribution is modified after Audebaud et al. (1973), Mégard (1978), Fontboté (1990), and Rosas (1994). The tectonic and structural framework is based on regional exploration data (INGEMMET, 1999; Tankard, 2001; PARSEP, 2002; PeruPetro proprietary files). The left-lateral sense of displacement on the major NNW-striking faults is interpreted from the overall pattern of subsidence and magmatism at releasing bends, shoaling on restraining jogs, and regional context. (b) Detail of outcropping Pucará sediments and relationship of outcrop to principal faults. Exploration seismic data show that these faults were used repeatedly during both basin formation and structural inversion, the most recent of which involved the Andean deformation. AB, Abancay; AR, Arequipa; AY, Ayacucho; CA, Cajamarca; CP, Cerro de Pasco; HSO, Huallaga stepover jog; HC, Huancayo; HV, Huancavelica; HU, Huánuco; LO, La Oroya; LI, Lima; LT, Lake Titicaca; OX, Oxapampa; TR, Trujillo.

sidence along the margin of the Brazilian shield, accompanied locally by volcanism along the steep, basin-forming faults. Furthermore, the facies tracts that typify the Pucará Basin fill reflect progressive marine flooding and enable us to correlate this inundation with other Andean basins.

2. Geological setting

Peru is divided into five tectonic domains that, not surprisingly, parallel the present Andean ranges (Benavides, 1999). The Andes formed by massive structural inversion and transpressional uplift of preexisting basins along their basin-forming faults. The upper Amazon Basin or Oriente region represents a Cenozoic foreland basin sandwiched between the Guyana-Brazilian shield, which it onlaps, and the Eastern Cordillera or Marañón Arch. In south central Peru, this jungle-covered lowland forms the Ene–Madre de Dios foreland basin, which subsided in front of a thin-skinned, fold-and-thrust belt and continues into northern Bolivia. Economically, this region is dominated by the giant Camisea gas-condensate field. The Western Platform spans the Western Cordillera and Altiplano of southern Peru. West of the cordillera is the topographic high of coastal Peru, sometimes referred to as the Divisoria Arch. Finally, the Mesozoic–Cenozoic subduction-related magmatic belt reveals presently active volcanism in northern and southern Peru. The present continental shelf faces an active subduction zone characterized by modern subduction earthquakes.

The Late Triassic–Middle Jurassic Pucará Basin of northern and central Peru straddles these NNW-oriented tectonic belts, from the Western Cordillera to the Oriente, and defines a pre-Andean landscape. It formed as a successor basin above a dissected and deformed platform of Permo-Carboniferous and Lower Triassic rocks (Fig. 2). The Upper Carboniferous and Permian Tarma–Copacabana succession consists of sandstones, mudstones, and limestones, the thickest parts of which were deposited in a suite of rifts linked to strike-slip fault zones. Fault-controlled subsidence gradually diminished and ceased by the Late Permian. Relaxation of the previous extensional basin-forming stresses resulted in widespread regional subsidence and formed a broad epeiric sea in which the argillaceous, organic-rich Ene Formation was deposited as a regional blanket or drape. The locus of postrift Ene subsidence was laterally offset to the east with respect to the previous fault-controlled phase of subsidence.

Reflection seismic data show that a pronounced unconformity intervenes between the deformed Ene and the overlying Mitu molasses. Fig. 3 shows these relationships, in which the seismic data have been restored to a prominent base-Cretaceous reflector (base of Sarayaquillo Formation). According to biostratigraphic well control, this pre-Mitu deformation is broadly dated as latest Permian–Early Triassic (G. Wine, pers. commun.), as is supported by radiometric dating of synkinematic granitic batholiths in the eastern Cordillera, with an age range of 255–236 Ma (Rb–Sr, K–Ar; Lancelot et al., 1978; Dalmayrac et al., 1980; Gunnesch et al., 1990; Soler, 1991). On the basis of seismic evidence of marked structural inversion in the Oriente region of Peru, Barros and Carneiro (1991) refer this latest Permian–Early Triassic episode of deformation to the Juruá orogeny. The Mitu redbeds were deposited in a suite of rift depocenters above the deformed Ene (Fig. 3) by a process akin to the orogenic collapse of Dewey (1988), following the Juruá orogeny.

The rift fill consists of terrigenous clastic molasse sediments, characterized by pronounced variations in thicknesses and facies over short distances, and alkaline volcanics of the Mitu Group, deformed within the Cenozoic fold-and-thrust belt of Peru and Bolivia (Mégard, 1978; Kontak et al., 1985; Mathalone and Montoya, 1995; Sempere et al., 1998, 1999). In the Oriente of Ecuador, reflection seismic data show that these depocenters are fault-bounded half graben structures (Balkwill et al., 1995). Mitu sedimentation was a response to strike-slip and associated extensional faulting; local discordances reflect pre-Pucará tilting. U/Pb geochronology of granodiorite batholith and detrital pebbles indicate the close relationship of the Mitu extension to the preceding Juruá orogeny, which suggests an Early Triassic age for the Mitu; detrital pebbles in Mitu conglomerates close to the San Vicente Mine are also Early Triassic (Fontboté and Gorzawski, 1990). Kontak et al. (1985) suggest a Middle Triassic age for the upper Mitu Group.

As fault-controlled subsidence of the Mitu extensional landscape gradually ceased, the various depocenters yoked together to form the broad epeiric Pucará Basin, expressed by widespread transgression of marine sediments that continued into the Late Cretaceous (Mégard, 1978; Benavides, 1999). However, the structural framework of the Mitu era persisted into the Pucará, though intermittently and with diminished intensity. The thickest parts of the Pucará are associated with principal NW-striking faults (Fig. 1), which we attribute to transtensional subsidence. The overall pattern of sedimentation and local volcanism at releasing bends, with thinning across right-stepping jogs between offset faults, indicate that the sense of displacement in the NW-trending basement faults was generally left-lateral (Tankard, 2001). Whereas the Mitu was characterized by widespread rift subsidence, the Pucará Basin was a regional sag in which local depocenters formed by intermittent transtensional subsidence (Fig. 1).

The Pucará cover consists of limestones, fine-grained organic-rich clastics, and evaporites. It terminates in the regional Sarayaquillo blanket of terrigenous clastics and evaporites along the cratonward margin (Figs. 4 and 5). The western margin of the Pucará Basin was a structural high (Fig. 1), the Divisoria Arch of Benavides (1999). The basin was connected to the ocean in the northwest, where there is some evidence of a volcanic arc. Recent work (LAGESA-CFGS, 1997) addressed the gradual transition along the eastern margin of Pucará carbonates into mixed clastic-evaporitic deposits (Lower Sarayaquillo

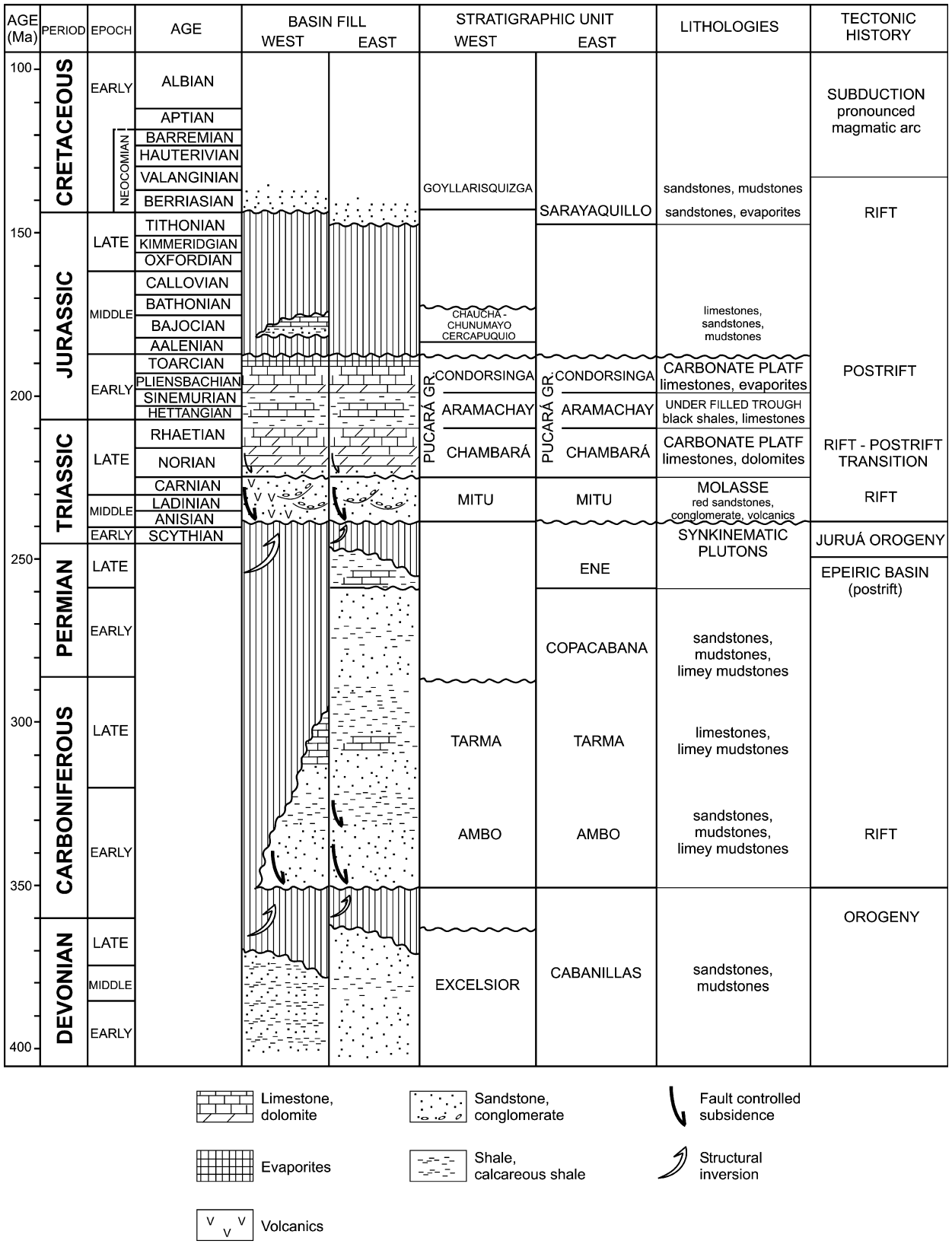

Fig. 2. Tectonostratigraphic column for the Pucará Basin. The Mitu rift system and postrift Pucará shown in relationship to the overall late Paleozoic–early Mesozoic history of basin evolution. A repetitive pattern of basin development and structural modification involved multiple phases of orogenesis, fault-controlled extensional subsidence, and decay or relaxation of extensional stresses, with each phase reworking preexisting basement structures to varying extents (Mégard, 1978; Mathalone and Montoya, 1995).

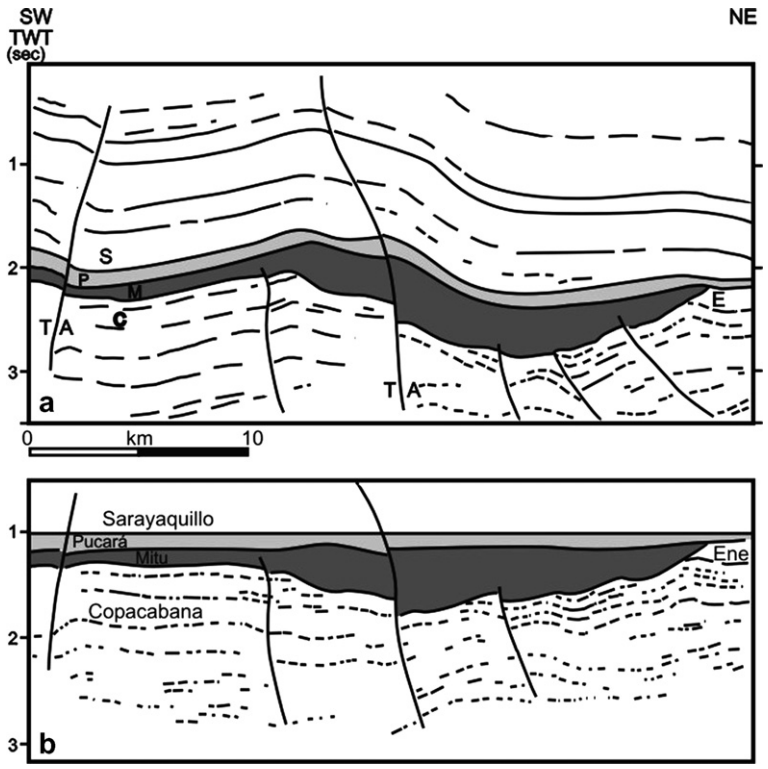

Fig. 3. Line drawing of reflection seismic data showing (1) Ene–Copacabana (C–E) stratigraphy deformed by the Juruá orogeny, (2) fault-controlled subsidence of the Mitu (M) rift system due to strike-slip associated extension, and (3) yoking together of the previous rifts to form the broad postrift epeiric basin of Pucará (P) time. The section is flattened at the base of the Sarayaquillo Formation (S). Interpretation courtesy of Gary Wine. Based on PARSEP (2002). TWT, two-way time.

Formation, Mégard, 1978). The Toarcian–Bathonian limestones of the Socosani Formation in southwestern Peru (Jenks, 1948; Benavides, 1962; Vicente, 1981) are also partly of Pucará age, but there is insufficient evidence to determine whether they were always isolated depocenters or once an integral part of the Pucará paleogeography.

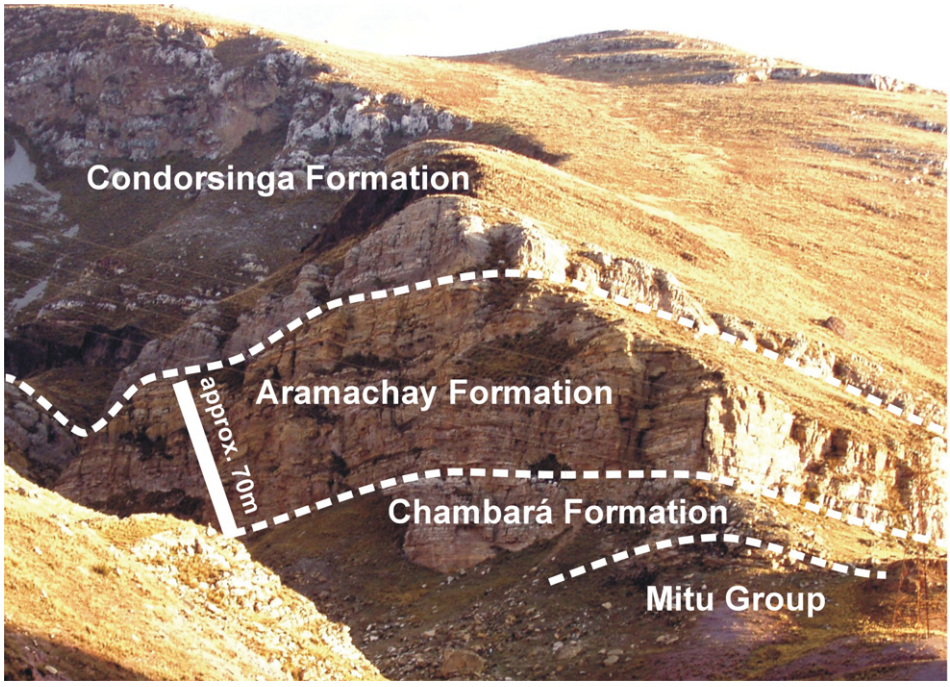

Fig. 4. Pucará succession in the Tingocancha area, site of a measured section. The Aramachay Formation is a ubiquitous drape of argillaceous material reflecting basin overdeepening between carbonate platform sediments below and above. Folding resulted from subsequent Andean deformation.

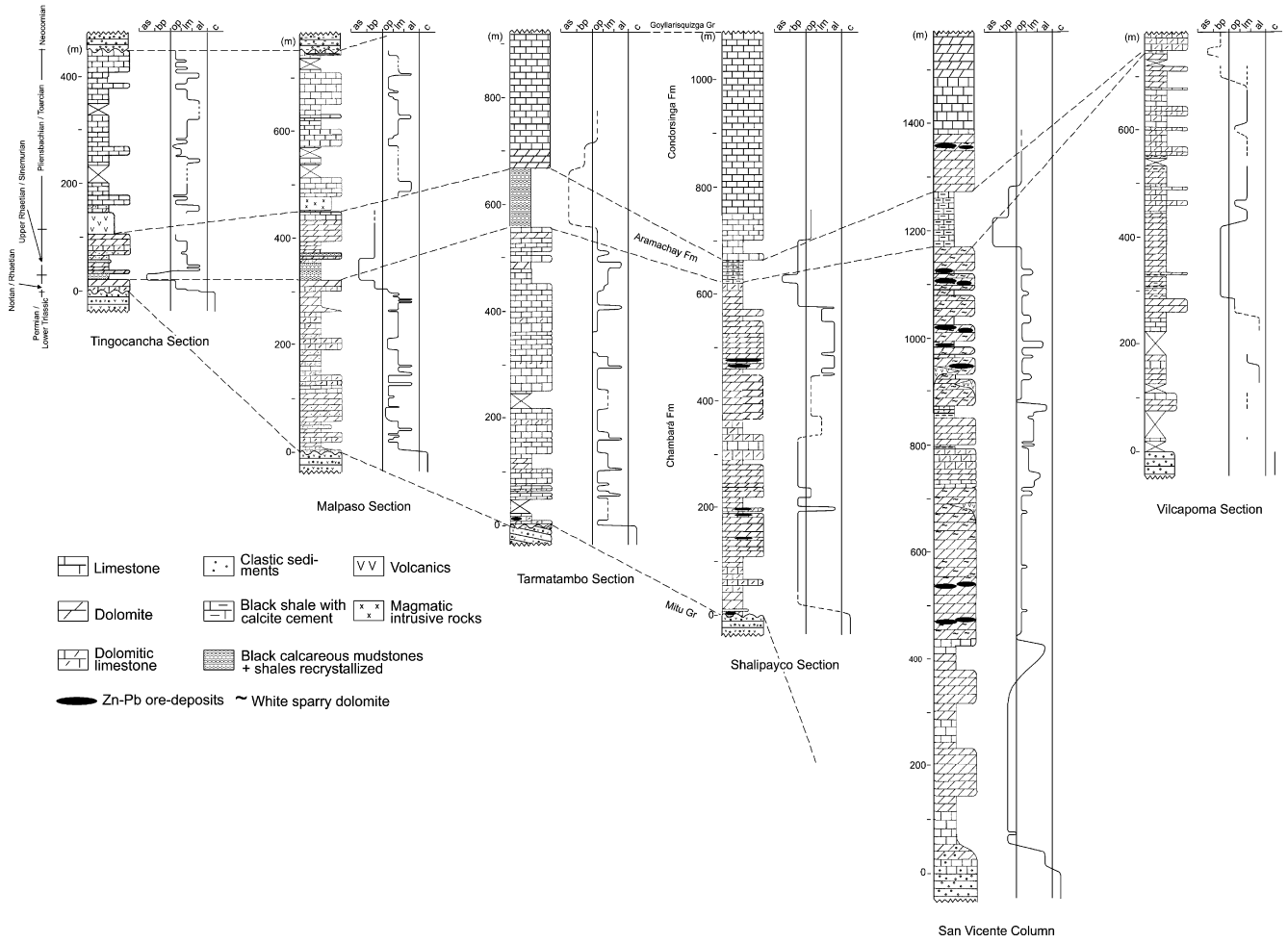

Fig. 5. Measured sections of the Pucará Group, showing lithologies and interpreted facies (see Rosas, 1994). The Shalipayco, San Vicente, and lower Tarmatambo sections are extensively dolomitized and have pods of Cenozoic-age MVT lead-zinc mineralisation associated with prominent strike-slip fault zones (Fig. 6). The western margin is a fault zone, and the Malpaso section is extensively dolomitized with sporadic tuffaceous interbeds. A summary of facies tracts is plotted on the right of each section. The principal facies and their interpreted paleoenvironments are as follows: *as,* ammonite-bearing, finely laminated anoxic black shales with high TOC content, interpreted as underfilled basin drape; *bp,* bioclastic packstones and wackestones forming 1–1.5 m thick lenses, attributed to traction sedimentation in the outer part of the tidal range as bioclastic shoals and bars; *op,* oolitic packstones and grainstones formed as shallow subtidal oolite banks and flats with local spillover lobes; *lm,* laminated mudstones with interbedded bioclastic wackestones and packstones and gypsum lenses, attributed to shallow subtidal carbonate flats with periodic desiccation; *al,* algal-laminated mudstones and evaporites with bird's-eye structures, geopetal structures, and wrinkled algal mats, attributed to intertidal and supratidal deposition.

In the Oriente Basin of Ecuador, seismic and well information record basement, fault-bounded, half-graben structures that contain hundreds of metres of conglomeratic, nonmarine, terrigenous clastics (Balkwill et al.,1995), a continuation of the Mitu paleogeography. In the Eastern Cordillera and Oriente Basin, these isolated rift segments are succeeded by a regional marine carbonate blanket, the Santiago Formation, of Pucará affinity (Fig. 1) (Geyer, 1980; Baldock, 1982; Balkwill et al., 1995). A marine transgression of Norian age also flooded the basins of Colombia, now recorded in the Payandé carbonates and volcanic-carbonate Saldaña Formation (Geyer, 1979, 1980; Cediel et al., 1981). A Liassic transgression is interpreted from the argillaceous and locally volcanic Morrocoyal and Batá formations. Northern Chile also reveals evidence of Late Triassic marine inundation as the sea progressively flooded a coast-parallel basin (Chong and Hillebrandt, 1985; Hillebrandt et al., 1986).

In summary, the western continental margin of South America has a remarkably similar record of marine inundation and deposition of terrigenous clastics, carbonate sediments, and associated basic volcanic rocks. Field studies and petroleum exploration show that flooding and sedimentation were accommodated by fault-controlled subsidence along the continental margin, and the similar timing indicates broadscale tectonic linkage of these extensional and strike-slip basin tracts.

In Peru, basic volcanic rocks occur sporadically throughout the Pucará succession (Rosas, 1994; Kobe, 1995). There is direct evidence of Late Triassic volcanic activity in the Chambará Formation in the central parts. These extrusives (Table 1) consist of alkaline olivine basalts

Table 1
Geochemiistry of intercalated volcanics

Unit	Chambará Fm Triassic		Aramachay Fm Hettangian-Sinemurian						Montero Suite in Condorsinga Fm Pliensbachian–Toarcian				
Locality	Lircay		Shalipayco						Yauli Dome				
Sample	HU-17	HU-23	35196	35197	35198	35234	35235	35258	PB-51	PB-53	PB-54	PB-55	PB-56
			Extrusives			Intrusives							
			wt%										
SiO_2	46.36	47.01	45.70	45.60	48.20	38.70	43.80	45.60	53.55	53.71	51.55	53.47	41.78
TiO_2	2.64	2.19	2.64	2.76	2.58	3.50	2.22	1.56	2.23	1.76	2.26	2.30	2.16
Al_2O_3	14.76	15.16	14.30	14.90	14.00	11.10	12.60	15.80	13.94	10.60	13.81	14.10	13.71
Fe_2O_3	10.88	10.21	9.63	4.70	9.62	14.00	9.31	7.44	11.78	8.37	15.54	11.68	10.36
MnO	0.21	0.15	0.06	0.06	0.08	0.18	0.09	0.05	0.14	0.06	0.18	0.18	0.16
MgO	6.43	6.62	2.46	0.74	3.83	8.79	3.45	5.11	4.12	0.14	3.55	4.10	2.04
CaO	7.90	9.30	12.90	16.10	11.10	9.78	13.10	9.95	6.54	10.26	5.35	6.33	11.37
Na_2O	4.05	3.02	3.25	3.47	3.24	1.15	1.24	2.91	3.00	5.02	4.04	3.76	4.41
K_2O	2.06	1.73	0.78	1.36	0.56	3.75	2.36	1.78	2.21	1.63	2.53	1.78	1.79
P_2O_5	na	0.93	0.32	0.30	0.33	1.14	0.30	0.37	0.57	0.40	0.51	0.37	0.31
Cr_2O_3	na	na	0.03	0.03	0.04	0.03	0.06	0.04	na	na	na	na	na
LOI	4.50	2.73	8.25	10.20	5.55	6.10	9.20	9.45	2.42	8.11	1.2	1.50	10.64
TOTAL	99.79	99.05	100.32	100.22	99.13	98.22	97.73	100.06	100.50	100.06	100.52	99.57	98.73
			ppm										
Ba	384	732	67	108	125	388	72	172	427	194	427	381	302
Rb	22	34	17	26	11	47	30	39	67	29	54	46	30
Sr	157	963	349	437	447	1070	229	394	200	96	352	333	114
Zr	186	217	159	164	165	292	117	158	301	244	193	212	198
Nb	na	50	12	11	15	74	14	13	14	13	8	9	bdl
Y	na	27	22	23	23	23	20	23	59	47	47	54	36
V	na	188	na	na	na	na	na	na	376	312	420	435	422
Co	na	40	na	na	na	na	na	na	56	24	65	59	31
Ni	na	419	na	na	na	na	na	na	11	bdl	12	17	bdl
Cr	na	294	na	na	na	na	na	na	20	13	19	19	24
Pb	na	118	na	na	na	na	na	na	7	22	6	4	bdl
Zn	na	113	na	na	na	na	na	na	95	105	70	78	64
Cu	na	49	na	na	na	na	na	na	49	70	12	17	bdl
La	na	32	na	na	na	na	na	na	20	13	15	10	30
Ce	na	91	na	na	na	na	na	na	56	44	39	41	51

Notes: Lircay and Yauli dome samples analysed at Mineralogy Laboratory, University of Geneva; Shalipayco samples at X-Ral, Canada. bdl, below detection limit; na, not analyzed; LOI, lost on ignition.

at Lircay (Rangel, 1978; Mégard et al., 1983; Morche and Larico, 1996) and local tuffaceous layers within the lower Pucará at the Yauli dome (Dalheimer, 1990). Younger intercalations of basaltic and andesitic flows occur within the Aramachay Formation at Shalipayco (Muñoz et al., 2000) and at the Yauli dome, where a 40 m thick interval of lava flows (the so-called Montero basalt) intercalates within the Condorsinga carbonates. The Yauli extrusives appear to have taken advantage of dilation at a releasing bend along a NW-oriented shear zone (Fig. 1b). We encountered thin layers of acid tuffs in the Malpaso and Tingocancha sections as well. Geochemical studies of the Shalipayco (Muñoz et al., 2000) and Montero extrusives, including whole-rock and trace element analyses, indicate an alkali to andesitic basalt composition with intraplate affinities (Rosas, 1994; Rosas et al., 1996, 1997), which may reflect transtensional dilation along steep, crustal-scale faults (see Sempere et al., 2002).

In contrast, the geochemical characterization of Liassic magmatic rocks in northwestern Peru indicates a volcanic arc setting (Pardo and Sanz, 1979; Prinz, 1985a; Romeuf, 1994; Romeuf et al., 1995); these are the Colán calc-alkaline basalts. At the other extreme, Lower Jurassic volcanic rocks of the Chocolate Formation occur in southern coastal Peru (Benavides, 1962; James et al., 1975; Vicente et al., 1982; Boily et al., 1984); they are 900–3000 m thick and consist of andesites, subordinate dacites, volcanic agglomerates, and breccias attributed to the early stages of volcanic-arc activity.

The Pucará phase of basin formation and sedimentation was caught up in the intense Andean (Late Cretaceous and Cenozoic) deformation, which involved both massive transpressional inversion driven by left-lateral strike-slip processes and thin-skinned structural shortening (e.g., Ene–Madre de Dios Andes; Tankard et al., 2006). Flat-slab subduction of the Nazca plate contributed to this tectonic behaviour and explains the distribution of younger volcanism (e.g., shoshonites close to the Brazilian border). (For a discussion of the kinematics of the Nazca plate, see Pilger, 1981, 1983; Gutscher et al., 1999.) Investigation of the Pucará requires some pre-Andean reconstruction, which locally involved seismic restoration of reflection seismic data (Fig. 3). Reflection seismic data show that the principal basin-forming structures were repeatedly reactivated and eventually accommodated Andean deformation itself.

3. Pucará: Triassic–Jurassic subsidence

The Pucará Group is dominated by shallow-water platform carbonates, except for an intermediate unit of bituminous calcareous shales that indicate deeper-water circulation. This threefold subdivision (Figs. 4 and 5) (Mégard, 1968; Szekely and Grose, 1972; Rosas and Fontboté, 1995) reflects intermittent basin subsidence and clearly facilitates stratigraphic correlation throughout the basin. First, the Chambará Formation (Norian–Rhaetian) consists of dolomite and subordinate limestone. Second, above it, the Aramachay Formation (upper Rhaetian–Sinemurian) of bituminous calcareous shales indicates an underfilled basin stage and deepening. Third, the Condorsinga Formation (upper Sinemurian–Toarcian) that caps the succession is again dominated by shallower-water limestone. Mégard (1968) and Stanley (1994) discuss the ages of this stratigraphy in detail. Our field investigation does not support an alternative sixfold subdivision of the eastern Pucará (Palacios, 1980).

The isopach reconstruction of Pucará is relatively well constrained in the area addressed by Fig. 6 and Table 2. Elsewhere, field exposure and well control is too limited to palinspastically restore the geology to a pre-Andean state or reconstruct reliable isopachs. The succession generally varies in thickness between 700 and 1500 m, except in the fault-bounded depocenters Cerro de Pasco, Oxapampa, and Huancayo, where greater thicknesses vary between 2200 and 2900 m. The elongate isopach distributions and rapid changes in thickness reflect transtensional subsidence along contemporaneous strike-slip faults.

3.1. Lithology of the Pucará Group

This description addresses the overall lithological makeup of the Pucará rocks in the various measured sections (Fig. 5) but emphasizes the Malpaso section, which is the most representative. Fig. 7 and Table 3 show the

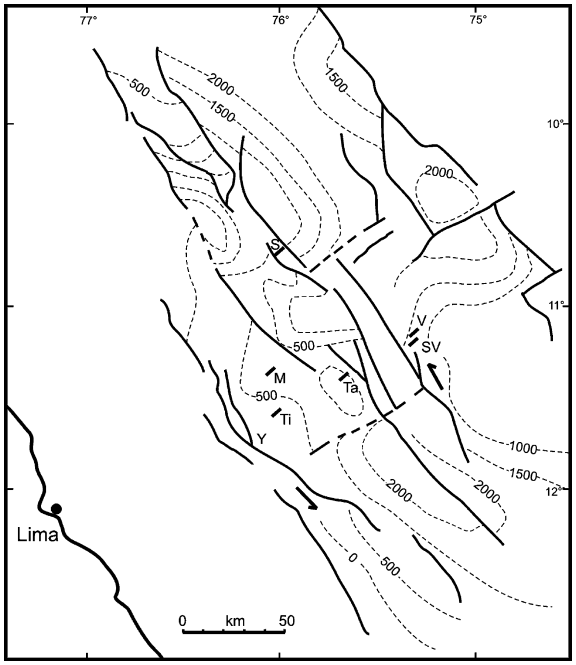

Fig. 6. Isopach distribution of the Pucará Group in the study area (see Table 2 for controls). Subsidence particularly pronounced along NNW-trending, strike-slip faults and NE-striking antithetic faults that form sidewall faults to local depocenters. Intersecting structures compartmentalized the basin. M, Malpaso; S, Shalipayco; SV, San Vicente; Ti, Tingocancha; Ta, Tarmatambo; V, Vilcapoma; Y, Yauli. Contours in meters.

Table 2
Localities and measured thicknesses of Pucará units

Locality	Coordinates	Chambará Fm. thickness (m)	Aramachay Fm. thickness (m)	Condorsinga Fm. thickness (m)	Pucará Gr. thickness (m)	Author
Aramango	5°20′S, 78°29′W	450	350	200	1000	De la Cruz (1995)
Ñaupe	5°43′S, 79°38′W	nd	nd	nd	700	Reyes and Caldas (1987)
Levanto	6°06′S, 77°52′W	350(?)	1390(?)	160(?)	1900	Sánchez (1995)
Río La Leche	6°27′S, 79°37′W	595	nd	nd	1240	Pardo and Sanz (1979)
Río Utcubamba	6°33′S, 77°44′W	450	150	80	680	Prinz (1985a)
C° Calvario	9°05′S, 76°53′W	>100[a]	nd	nd	nd	Jacay (1996)
5 km N of Tingo María	9°16'S, 76°01'W	nd	nd	nd	~2200	Dávila et al. (1999)
40 km S of Aguaytia	9°24′S, 75°34′W	nd	nd	nd	~1200	Dávila et al. (1999)
16 km SE of Tingo María	9°27'S, 75°57'W	nd	nd	nd	~2000	Dávila et al. (1999)
38 km SE of Tingo María	9°37′S, 75°52′W	nd	nd	nd	~2300	Dávila et al. (1999)
Tambo de Vaca	9°54′S, 75°49′W	nd	nd	nd	~1720	Dávila et al. (1999)
16 km SW of Pozuzo	10°11′S, 75°36′W	nd	nd	nd	~1650	Dávila et al. (1999)
23 km WSW of Ambo	10°13′S, 76°23′W	nd	nd	nd	~400	Dávila et al. (1999)
Iscozacín (DDH)	10°13′S, 75°10′W	nd	nd	nd	700	Dávila et al. (1999)
10 km WSW of Goyllarisquizga	10°32′S, 76°29′W	nd	nd	nd	~480	Dávila et al. (1999)
Atacocha-Chicrín area	10°36′S, 76°14′W	nd	nd	nd	2100	Szekely and Grose (1972)
Huachón	10°37′S, 75°57′W	nd	nd	nd	>700	Dávila et al. (1999)
2–8 km E of C° de Pasco	10°42'S, 76°17'W	nd	nd	nd	2931	Szekely and Grose (1972)
7 km W and SW of C° de Pasco	10°43′S, 76°20′W	nd	nd	0(?)	627	Szekely and Grose (1972)
6 km W of Tambo María	10°43′S, 75°25′W	nd	nd	nd	~1680	Dávila et al. (1999)
Tambo María	10°43′S, 75°22′W	nd	nd	nd	~1700	Dávila et al. (1999)
Oxapampa	10°46′S, 75°17′W	1600	350	800	2750	Palacios (1980)
Shalipayco	10° 50′S, 75°58′W	622	40	>93	>1050	This work
5 km WNW of Raymondi Sur	10°53′S, 75°26′W	nd	nd	nd	~2100	Dávila et al. (1999)
Carhuamayo	10°54′S, 76°04′W	nd	nd	nd	~1050	Dávila et al. (1999)
Quebrada Zutziki	10°54'S, 74°57'W	nd	nd	nd	>1500	S and Z Consultores (1997)
6 km WNW of Pucapaccha	10°56′S, 75°56′W	nd	nd	nd	>1250	Dávila et al. (1999)
2 km NE of Huaire	10°58'S, 76°02'W	1700	nd	nd	>1700	Szekely and Grose (1972)
Satipo	11°00′S, 74°49′W	nd	nd	nd	>1190	LAGESA-CFGS (1997)
Vilcapoma		730	10	~60	~800	This work
San Vicente	11°12′S, 75°21′W	1170	105	>250	>1550	This work

(*continued on next page*)

Table 2 (*continued*)

Locality	Coordinates	Chambará Fm. thickness (m)	Aramachay Fm. thickness (m)	Condorsinga Fm. thickness (m)	Pucará Gr. thickness (m)	Author
7 km WSW of Ondores	11°07′S, 76°12′W	nd	nd	nd	~350	Dávila et al. (1999)
Piñón	11°21′S, 75°21′W	nd	nd	nd	>1000	Dávila et al. (1999)
Malpaso	11°25′S, 76°01′W	319	125	303	747	This work
9 km S of Tarma	11°29′S, 75°40′W	nd	nd	nd	~1000	Dávila et al. (1999)
Tarmatambo	11°28′S 75°42′W	557	~90	>50	>900	This work
Huaricolca	11°31′S, 75°47′W	430	100	270	800	Senowbari-Daryan and Stanley (1986)
E of Inca Tacuna	11°31′S, 75°31′W	722	391	1200	2313	Szekely and Grose (1972)
Morococha	11°37′S, 76°09′W	nd	nd	nd	431	Szekely and Grose (1972)
Tingocancha	11°37′S, 75°59′W	25	73	354	452	This work
San Pablo	11°40′S, 75°33′W	nd	nd	nd	~2100	Dávila et al. (1999)
Yauli-San Cristóbal area	11°42′S, 76°06′W	nd	108	113	221	Szekely and Grose (1972)
Jauja	11°43′S, 75°21′W	355	300	>>154	>>800	Paredes (1994)
8 km S-SW of San Cristóbal	11°48′S, 76°07′W	nd	nd	nd	509	Szekely and Grose (1972)
Huancayo	12°03′S, 75°14′W	600	408	1200	2208	Loughman and Hallam (1982)
Anticlinal de Quintojo	12°11′S, 74°28′W	nd	nd	nd	>1467	Guizado and Landa (1966)
Lircay	12°58′S, 74°42′W	±400	100	±500	±1000	Rangel (1978)

[a] Strong erosion of upper Pucará; nd, not determined.

results of the petrographic examination of 431 thin sections and XRF analyses of 157 whole-rock samples (see also Rosas, 1994; Rosas and Fontboté, 1995).

The Chambará Formation is predominantly dolomitic (>80%) with locally interbedded calcareous dolomites and limestones. Although these dolomite-prone lithologies are widespread, they are particularly associated with outcrops along the intrabasinal shear zones (Fig. 1b). In contrast, the Chambará in the Tarmatambo section at mid-basin consists exclusively of limestone. The detrital content varies up to 30%, mainly in the lower part of the sequence, with average values of 12 wt% SiO_2 and 2 wt% Al_2O_3. Detrital quartz is least abundant at Tarmatambo and Shalipayco. Chert is ubiquitous in the Chambará Formation and occurs as centimeter-scale bands and nodules. Other common macroscopic components include carbonate pseudomorphs after gypsum and anhydrite, burrow casts, macrofossils (bivalves, gastropods, crinoids, ostracods, and brachiopods), algal mats, and bird's-eye textures. Laminar bedding is common in the mudstones, and cross-bedding occurs in the grainstones.

In contrast to the other sections, the basal Pucará at San Vicente shows a gradual transition from clastic red silt and sandstone facies with evaporite intercalations (Dávila et al., 1999) that resemble the upper Mitu. Mégard (1978) and Fontboté and Gorzawski (1990) refer this "Red Sandstone" to basal Pucará facies, rather than Mitu, but acknowledge that the absence of an angular unconformity and the gradual lithological change makes it difficult to distinguish between the two.

The Aramachay Formation is dominated by black argillaceous limestones and shales, compared with the Chambará below or Condorsinga above, and is thus less well exposed. However, the Aramachay at Tingocancha and Malpaso is unique because mild contact metamorphism and volcaniclastic material has helped lithify the argillaceous sediments (illites, variable amounts of calcite, and abundant chert), making the sedimentary succession more robust. There is also less organic material in these outcrops, probably because basin-margin uplift and oxidation depleted the carbon content. The upper part of Aramachay at Tingocancha and Malpaso is strongly dolomitized and includes distinctive recrystallized argillaceous lithologies. Lithogeochemistry provides an invaluable tool to characterize the Aramachay Formation. In each column, the lower part of the Aramachay Formation is distinguished

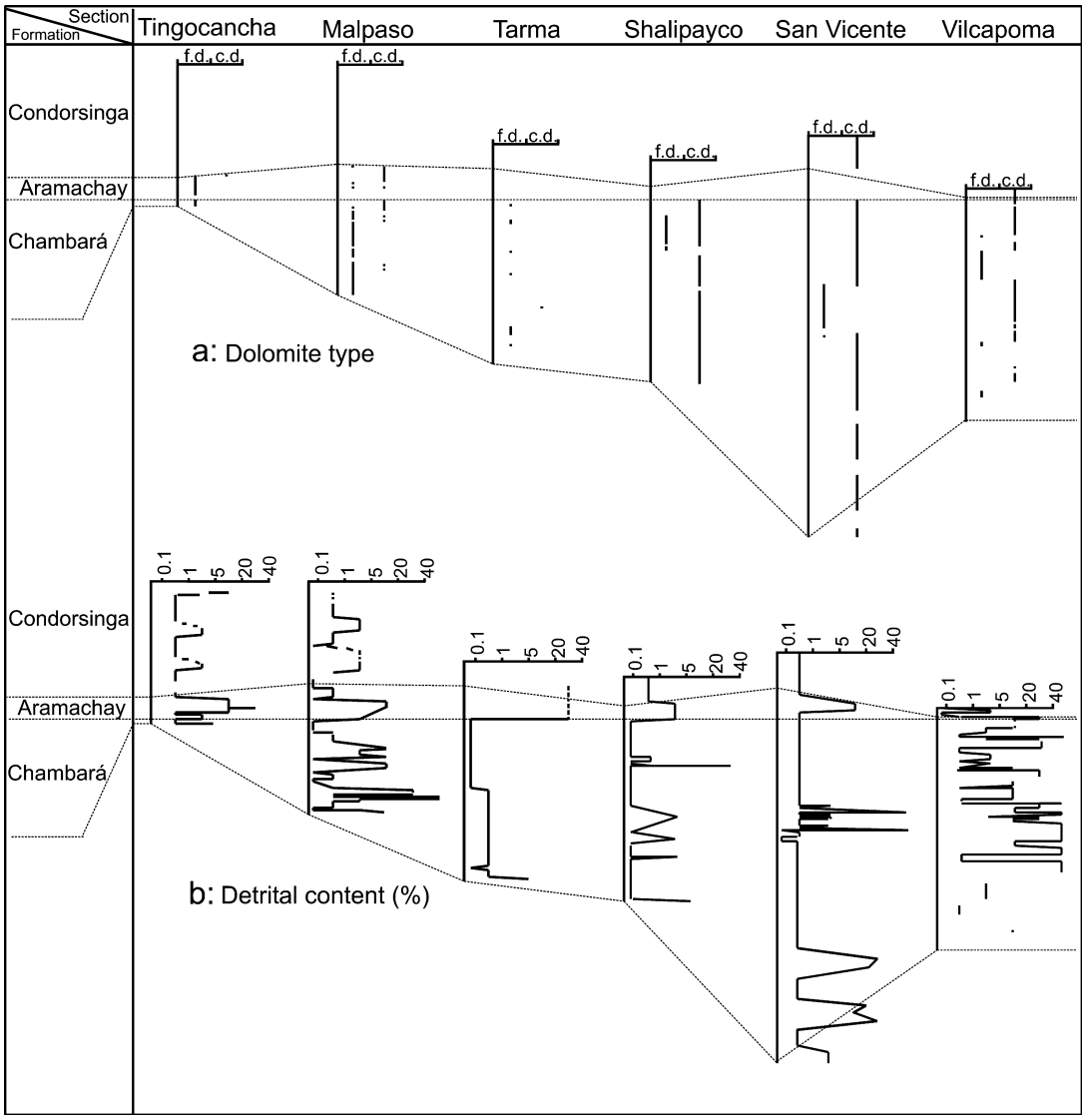

Fig. 7. Comparison of dolomite type and detrital content of each measured section. fd, finely crystalline dolomite; cd, medium to coarsely crystalline dolomite.

by higher SiO_2, Al_2O_3, TiO_2, and K_2O contents than the underlying and overlying Chambará and Condorsinga formations (Fig. 8 and Table 3).

This field investigation has mapped Aramachay sediments at Shalipayco. In the eastern part of the basin, near the San Vicente and Pichita Caluga mines, the bituminous silty limestones of the Aramachay Formation are conspicuous and known locally as the Uncush limestone (Dávila et al., 1999).

The Condorsinga Formation is limestone dominated but differs from the Chambará platform succession in that it has far less dolomitization that, where present, is restricted to the lower parts of the unit (Fig. 7). Chert is also less abundant, and the quartz-prone detrital content is less than 3%. However, in the more marginal San Vicente area, there are conspicuous silty-argillaceous intercalations within the Condorsinga carbonates (Arcopunco limestone of Dávila et al., 1999).

3.2. Stratigraphic framework

The six stratigraphic columns examined in detail are shown in Fig. 5; the total outcrop surveyed exceeds 4800 m. Whereas the Chambará and Aramachay formations are present and fully exposed in all six measured sections, the overlying Condorsinga Formation occurs only in the Tingocancha and Malpaso columns. Elsewhere, Andean-age structural inversion and erosion have stripped the Condorsinga. The Pucará succession has a disconformable to angular unconformable relationship with the underlying Mitu (contact is an angular unconformity at Tarmatambo) and is separated from the overlying sandstones and siltstones of the Lower Cretaceous Goyllarisquizga Group by sharp contact. Because of their limited appreciation of the sedimentary facies, previous studies (e.g., Harrison, 1943; Szekely and Grose, 1972) have failed to recognize Chambará rocks in the Yauli dome area.

Table 3
Geochemical characterization of Pucará succession

Unit	Chambará					Aramachay							Condorsinga			
Section	Tingocancha	Malpaso	Tarma	Shalipayco	San Vicente	Tingocancha		Malpaso		Tarma	Shalipayco	San Vicente	Tingocancha	Malpaso	Tarma	San Vicente
						l.p.	u.p.	l.p.	u.p.							
						wt%										
CaO	30.70	32.01	47.94	34.01	32.75	17.46	23.26	9.38	24.32	0.89	15.68	28.28	39.93	49.84	0.36	29.00
MgO	17.03	13.68	4.17	16.08	16.36	10.58	12.67	4.74	14.95	0.59	0.92	1.77	8.67	2.63	0.24	19.30
SiO_2	7.94	12.04	4.78	4.84	3.67	36.17	21.95	61.45	20.44	77.30	48.28	35.56	7.92	3.79	96.50	9.10
Al_2O_3	0.76	1.34	0.35	0.40	0.82	6.83	4.76	6.70	2.78	8.92	6.43	4.32	0.88	0.59	1.30	0.73
Fe_2O_3	0.83	0.64	0.27	2.17	1.41	1.24	2.31	1.58	1.25	3.71	3.79	2.53	0.57	0.47	0.75	1.09
LOI	42.88	39.65	42.33	40.72	43.78	27.58	33.60	14.38	35.60	3.36	19.06	24.78	40.97	41.86	1.13	39.40
						ppm										
MnO	578	1955	99	3134	1178	474	305	294	333	251	300	620	557	147	bdl	1343
Na_2O	2787	2540	779	na	na	1808	1394	2130	2113	2300	600	1640	977	1101	266	na
K_2O	212	3021	989	1671	2093	1206	5957	9352	6478	40000	25500	11600	2189	952	1473	2024
TiO_2	281	508	227	518	44	1530	3312	3302	1543	5672	4600	2700	423	310	1077	55
P_2O_5	276	1462	980	2465	na	732	1036	3395	1250	8736	2100	4840	176	166	2481	na
Sr*	153	163	251	152	123	306	759	397	87	40	410	849	124	133	21	71
Ba*	bdl	150	35	92	31	306	bdl	969	bdl	108	43	67	bdl	bdl	bdl	na
Rb*	1	8	4	na	na	4	4	7	29	60	54	38	3	5	6	na
U*	1	1	3	na	na	3	bdl	5	1	3	14	5	1	bdl	bdl	na
La*	3	7	4	na	na	31	9	21	4	24	15	11	3	4	bdl	na
Ce*	26	23	23	na	na	62	31	46	22	38	28	31	19	24	bdl	na
Nd*	9	11	14	na	na	17	14	8	8	13	17	11	6	12	bdl	na
Y*	4	8	3	na	na	15	19	30	11	45	26	19	3	4	6	na
Zr*	12	13	7	na	na	151	68	107	51	176	124	85	bdl	bdl	22	na
V*	5	5	4	na	na	1	29	12	15	53	524	32	1	4	bdl	na
Cr*	7	18	7	na	na	16	12	35	22	65	130	168	7	3	121	na
Ni*	bdl	bdl	1	3	na	bdl	bdl	3	bdl	20	161	13	bdl	1	bdl	na
Co*	2	3	4	na	na	bdl	1	bdl	1	1	bdl	9	2	5	bdl	na
S*	1141	482	430	503	na	508	1031	182	528	271	5852	2838	462	434	96	na
Cu*	bdl	bdl	bdl	4	na	bdl	15	bdl	bdl	bdl	29	3	bdl	bdl	bdl	na
Zn*	145	220	27	1729	na	56	58	5	17	16	551	27	17	22	1	na
Pb*	41	19	2	na	na	10	17	14	4	30	10	5	2	1	bdl	na
						wt%										
Total	100.71	100.41	100.23	99.25	99.14	100.58	99.96	100.26	100.59	100.56	98.27	99.80	99.43	99.51	100.84	98.96
n_{wr}	13	32	6	34	75	12	11	6	6	1	1	5	13	16	1	1
n_{trace}	3	3	6	34	75	3	2	2	3	1	1	5	3	3	1	1

Notes: Analysed at Mineralogy Laboratory, University of Geneva.
n_{wr}, no. of whole rock samples; n_{trace}, no. of trace element samples; bdl, below detection limit; na, not analyzed; LOI, lost on ignition.
Whole-rock XRF analyses.

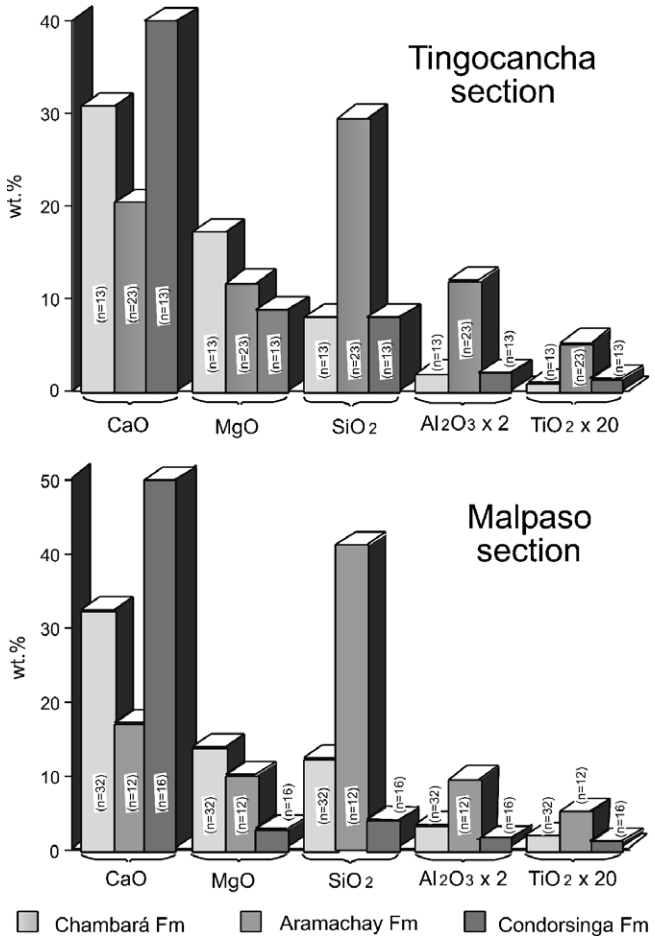

Fig. 8. Comparison of major elements between Tingocancha and Malpaso (see Table 3). Units at Tingocancha interpreted on the basis of the lithogeochemical similarities of the Chambará, Aramachay, and Condorsinga formations.

However, more recent work by Rosas (1994) on the Tingocancha column at the Yauli dome documents the shallow-water Chambará facies as well as the overlying deeper-water Aramachay facies with their characteristic lithogeochemistry (e.g., elevated SiO_2, Al_2O_3, and TiO_2 contents; Table 3). The marked thinning of the Chambará stratigraphy and its association with the Yauli volcanic rocks reflects basin-margin structural control; the extrusive and intrusive magmatism formed at a releasing bend where uplift caused stratigraphic thinning. The entire Pucará succession is also recognized at Shalipayco, including up to 665 m of typical ammonite-bearing Aramachay lithologies of early Sinemurian age (e.g., *Arnioceras*, Rosas, 1994, quoting Prinz). Aramachay argillites in the Malpaso column are confirmed by the late Sinemurian–Pliensbachian bivalve *Weyla alata* (Prinz, in Rosas, 1994) and the Triassic–Liassic microcoprolite *Parafavreina thoronetensis* (Blau et al., 1994).

3.2.1. Chambará formation: transitional postrift subsidence

The Upper Triassic limestones and dolomites exposed just north of Huancayo, near the village of Chambará, were assigned to the Chambará Formation by Mégard (1968). Its contact with the underlying Mitu is generally disconformable, except where pre-Chambará structural inversion has resulted in a slight angular discontinuity (see also Mégard, 1979; Szekely and Grose, 1972). The variation of thickness of this formation from 25 m at Tingocancha to 1180 m at San Vicente is ascribed to a structural control that persisted from the earlier Mitu rift phase. Lithologically, this formation is dominated by limestones and dolomites, and along the margins of the basin, reworking has resulted in a significant detrital component, locally exceeding 40% (Fig. 7).

A Norian–Rhaetian age for the Chambará Formation is established by the occurrence of the brachiopod *Spondylospira* sp. (Mégard, 1968), the bivalve *Monotis subcircularis* Gabb (Prinz, 1985b), and the microcoprolites *Palaxius salataensis*, *Parafavreina thoronetensis*, and *Parafavreina huaricolcanensis* (Senowbari-Daryan and Stanley, 1986).

3.2.2. Aramachay Formation: deep-water stage

Mégard (1968) named the Aramachay Formation to describe the organic-rich shaly carbonate rock he encountered southwest of the village of Aramachay. The Aramachay succession is dominated by laminated, bituminous black limestones that contain sporadic shaly and silty intercalations. This unit, which varies in thickness from 100 to 200 m, is more uniform than the underlying Chambará, suggesting it was deposited as a regional drape largely unaffected by fault activity. Together with ammonite and other diagnostic fossils, this argillaceous drape is attributed to deposition in a restricted marine environment. Total organic carbon (TOC) values range from 0.28 to 4.01 wt% (Spangenberg et al., 1999). The organic-rich sediments have relatively high phosphate values typical of high biologic productivity and reducing conditions in the sea-floor sediments. Loughman and Hallam (1982) report values up to 8.6 wt.% P_2O_5, and we determine up to 1 wt% P_2O_5 in the San Vicente column. Other associations include asphaltites that are abnormally high in vanadium (0.15–0.2% V), and selenium and uranium have been reported in the Sincos exposures (Fig. 1) (Larson and Welker, 1947; Szekely and Grose, 1972; Cánepa, 1990; Paredes, 1994).

A late Rhaetian–Sinemurian age for the Aramachay Formation is indicated by the ammonites *Vermiceras*, *Arnioceras*, *Eparietites,* and *Plesechioceras* (Mégard, 1968); *Psiloceras* (Prinz, 1985b); *Choristoceras* cf. *nobile* (Prinz, 1985a); and the mollusks *Aucella* and *Cucullaea* (Mégard, 1968; see also Stanley, 1994). The presence of the late Rhaetian ammonite *Choristoceras* cf. *nobile* in the Utcubamba Valley of northern Peru (Prinz, 1985a) shows accumulation of Aramachay sediments.

3.3.3. Condorsinga Formation: carbonate platform

Carbonate platform sediments above the Aramachay argillaceous limestones in the Jatunhuasi area are referred

to the Condorsinga Formation by McLaughlin (1924). These strata consist mostly of limestones, but dolomite occurs locally at the base of the succession in some places. Together with intraformational gypsum lenses, which have been exploited commercially in the Yauli and Malpaso areas, a shoal-water and largely overfilled basin setting is envisaged. The Condorsinga succession is not present everywhere because subsequent deformation and erosion stripped it. Thus, regional thickness estimates are largely unknown, though we measure thicknesses of 300–350 m.

The fossil assemblages include *Oxynoticeras*, *Coeloceras*, *Androgynoceras*, *Uptonia*, *Phymatoceras*, *Esericeras*, *Arititidaes*, *Pentacrinites* sp., *Phaenodesmia* sp., *Weyla alata*, *Trigonia inexpectata*, *Arieticeras* sp., and *Ctenostreon* sp. (Pardo in Mégard, 1968; Palacios, 1980). The presence of the ammonites Phymatoceras and Esericeras (Mégard, 1968) in particular suggest a late Toarcian age, at least for the upper part of the Condorsinga Formation (see also Stanley, 1994). The new microcoprolite species *Favreina peruviensis* has been identified in the Condorsinga Formation at both Tingocancha and Malpaso (Blau et al., 1994).

4. Pucará paleogeography

4.1. Depositional systems

The Pucará Group generally overlies the Mitu with a paraconformable contact, although at Tarma and Shalipayco the contact is an angular unconformity. An abrupt lithological change occurs from purple volcaniclastic sediments below to a gray dolomite above, with detrital content up to 40% (Fig. 7). Fig. 5 displays the lithologies and sedimentary facies in several measured sections. The Chambará succession consists of 0.3–5.0 m thick layers of dolomite and subordinate marly dolomites with interbedded calcareous dolomite and sparse limestone. A greater amount of quartz-prone detrital material (up to 30%) dilutes the carbonate lithologies in the western and eastern sections. We attribute the greater detrital content in the west to reworking along the basin margin; that in the east may be due to local uplift and the proximity of continental clastic influx from the neighboring Guyana–Brazilian shield. Bedded and nodular chert, bivalves, and crinoids, as well as burrows, are abundant. Hard-grounds occur near the top of this formation. Wavy and horizontal lamination and carbonate pseudomorphs after gypsum or anhydrite are observed in the mudstones. The coarser-grained beds are cross-laminated.

The transition to postrift Chambará subsidence and deposition is marked by sedimentary facies that appear to represent the basinward tracts of a tidally influenced succession. At San Vicente, gypsum and redbeds mark the Mitu–Pucará transition and are interbedded with the overlying carbonates. In the northeastern part of the study area, the Oxapampa 7-1 exploration well penetrates 1800 m of interbedded carbonates and evaporites. Most commonly, the sediments near the base of the Chambará are characterized by bioclastic material that diagnoses an unrestricted, open basin circulation, such as a modern marine shelf. Above, the Chambará lithofacies are attributed to subtidal processes, as might be encountered in a more restricted back-barrier or lagoonal setting, whereas other less common facies have intertidal and supratidal affinities. These lithofacies associations may be grouped into four distinct sedimentary sequences. The lower three characteristically have shallowing-upward tendencies with a preponderance of subtidal facies in the lower parts, and shallower facies associations become increasingly more abundant upward. The subtidal to intertidal lagoon-type facies consist typically of laminated dolomitic mudstones, bioclastic and peloidal wackestones and packstones, and grapestones (Fig. 9a–d), all of which are commonly rimmed with early diagenetic submarine cements. Oncolites, pellets, intraclasts, and bioclasts of bivalves and foraminifers are common among the agglutinated components of the grapestones. The oolitic and bioclastic grainstones (Fig. 9c) are diagnostic of traction sedimentation across shoal-water bars and channelized environments. Locally, they have early diagenetic submarine cements. In this setting, the subtidal oolitic banks are associated with laminated lagoonal sediments. Elsewhere, this transition is marked by grapestone facies or a progressive increase in the typical lagoonal facies components (e.g., pellets, bioclasts, micrite).

Other facies are interpreted as intertidal and supratidal. They are mainly argillaceous and contain algal mats, bird's-eye structures, and breccias. Furthermore, sabkha-type facies with algal mats and early diagenetic, finely crystalline dolomite also occur in the upper part of the shallowing-upward sequences, where they are associated with intertidal facies that contain desiccation fabrics (Fig. 9e) and evaporite pseudomorphs. A variant of the bird's-eye fabrics are geopetal features in which the internal cement recrystallized during diagenesis (Fig. 9f); these geopetal structures occur in massive (i.e., unstructured) argillaceous sediments that cap some tidal facies.

The uppermost cycle exposed at Malpaso represents a return to the open basin circulation that marked the initiation of Chambará deposition. These interpreted depositional banks are composed of strongly dolomitized crinoid-bioclastic packstones (Fig. 9d) and subordinate, siliceous sponge, spicule-rich wackestones. Pervasive dolomitization is accompanied by extensive porosity development. Later-stage intercrystalline calcite- and kaolinite–cement is common. Hard-ground surfaces are abundant at the top of this cycle, capping the succession of crinoidal banks and the deeper basin facies of chert-cemented bioclastic packstones with abundant iron oxide impregnations. These characteristics are interpreted as a sedimentary hiatus that may mark the transition to a new stage of rapid basin deepening of the Aramachay milieu.

The Aramachay Formation is 125 m thick at Malpaso (Fig. 5). There and at Tingocancha, it contains two lithological units. The lower 40 m consists of 0.20–0.5 m thick,

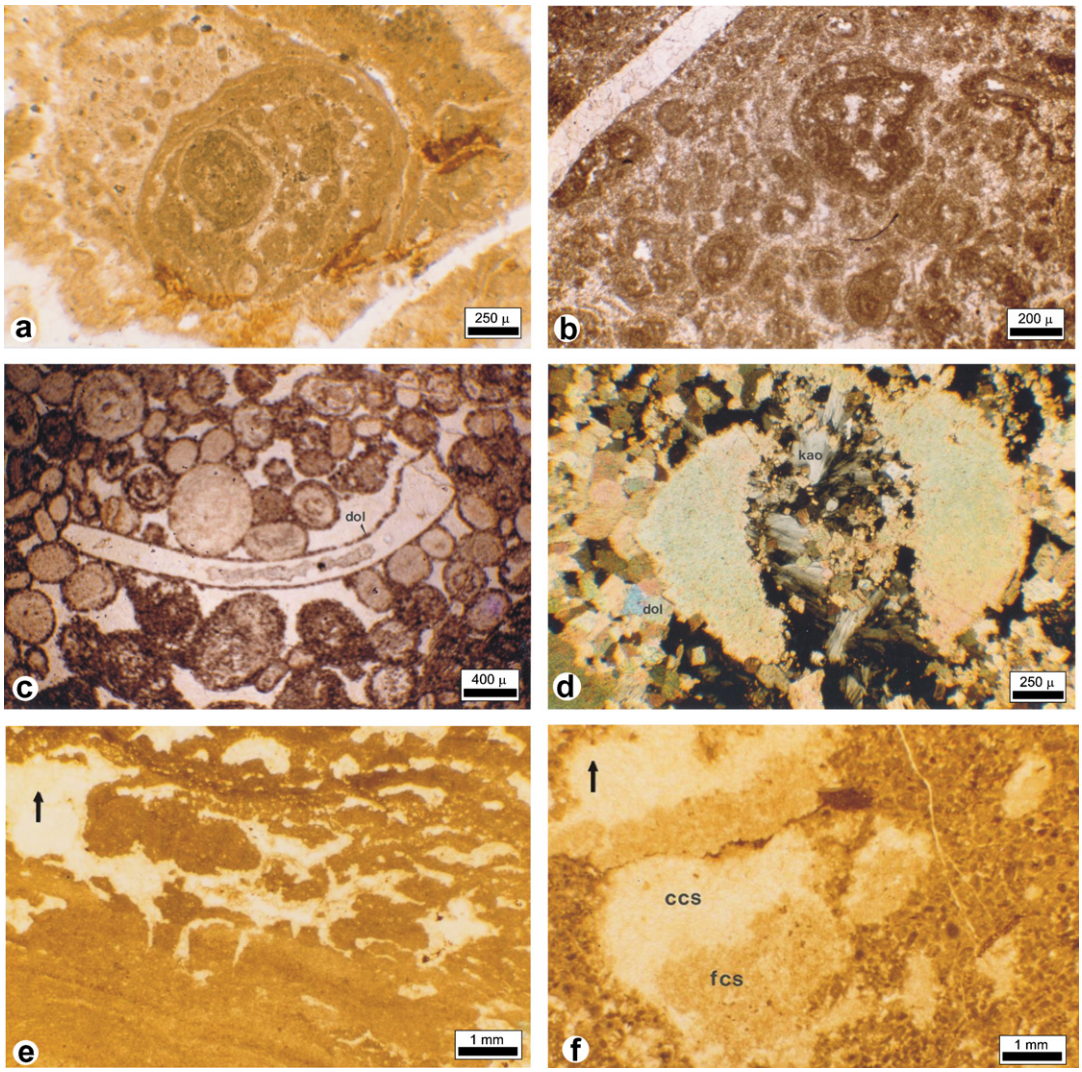

Fig. 9. Representative microscopic photographs of Chambará facies in Malpaso section. (a) Grain of grapestone, the agglutinated components consisting of smaller particles and pellets (25 m above Mitu datum). (b) Grapestone, agglutinated components partially dissolved and cemented peloids (25 m above Mitu). (c) Strongly chertified oolitic grainstone with bioclasts, mainly bivalve fragments, dolomitic early diagenetic cement (dol) at the allochem borders (138 m above Mitu). (d) Bioclasts from a crinoid bank, dolosparite (dol) and kaolinite (kao) as cement (crossed nicols; 314 m above Mitu). (e) Finely crystalline dolomite, probably early diagenetic, algal mat with bird's-eye porosity, cemented by a first-generation dolomitic cement; facies occurs directly on top of subtidal facies (280 m above Mitu). (f) Bird's-eye porosity filled with geopetal cement and consisting of finely crystalline sparite (fcs) replacing internal sediments and coarsely crystalline sparite (ccs) filling empty spaces; the petrographic texture corresponds to a micritized peloidal and oolitic grainstone; facies overlies subtidal facies (32 m above Mitu).

dark-brown layers of strongly recrystallized argillaceous carbonate sediments that are locally chert rich. Recrystallization reflects weak contact metamorphism that was, in places, sufficient to mask the original facies. High values of TiO_2, Al_2O_3, K_2O, and TiO_2 (Fig. 8; Table 3) match the abundant clay mineral content and probably result from volcanic activity. This interpretation is supported by the presence of several beds of volcanic tuffs in the upper part of the Aramachay. Overall, the Aramachay Formation is characterized by high organic material contents (TOC varies between 0.3 and 4.0 wt%; Mégard, 1968), and the lower part of the Aramachay Formation is interpreted as an underfilled, deep-water basin. It has the characteristics of an epeiric basin.

The upper Aramachay consists almost exclusively of 0.3–1.3 m thick layers of dolomite, with marly dolomites and chert occurring locally, and has interbeds of tuffs and limestones near the top. The altered tuffs and trace element data indicate an original dacitic to rhyodacitic composition. The predominant facies are bioclastic wackestones of sponge spicules, crinoids, brachiopods, and bivalves, as well as subordinate crinoidal bank facies, all of which resemble modern marine shelf sediments. Bedded and nodular cherts, as well as macrofossils of bivalves and crinoids, occur sporadically. The transition from the restricted basin facies of the lower Aramachay to this upper, less restricted, open basin-type accumulation is relatively sharp. This subdivision is observed only at Malpaso, and its absence

elsewhere may reflect poor exposure. However, a broadly similar, twofold subdivision of Aramachay sediments has been recognized in northern Peru (Chilingote and Suta units of Weaver, 1942) and central Peru (Ichpachi and Alata units of Loughman and Hallam, 1982).

Along the basin margin where the San Vicente and Vilcapoma rocks are associated with a splayed shear zone (Fig. 1b), sudden changes in thickness of the Aramachay from 8 to 250 m have been documented (Dávila et al., 1999), in part reflecting structurally controlled compartmentalization. According to Hasler (1998), where the Aramachay is extremely thin (i.e., 8–15 m), the presence of evaporite pseudomorphs suggests deposition took place in relatively shallow water, as indicated.

The Aramachay–Condorsinga contact at Tingocancha and Malpaso is marked by a decrease in the amount of volcaniclastic components and a sudden reduction in TiO_2 (Fig. 8 and Table 3). In the field, it is expressed as a conspicuous change in the weathering color from brown to light gray. In contrast, at Tarmatambo, Shalipayco, San Vicente, and Vilcapoma, the contact superimposes shaly carbonate rocks, limestones, and dolomites on organic-rich shaly carbonates. A sill of coarse-grained alkaline basalt occurs 10 m above the base of the formation at Malpaso. (Radiometric dating gives a latest Cretaceous Andean age of intrusion, 65 ± 2.9 to 70.8 ± 2.6 Ma, Rosas, 1994.) The contact with the overlying Goyllarisquizga Group is an erosional unconformity.

The Condorsinga lithofacies show a return to the type of paleogeography encountered in the lower part of the Chambará Formation, especially alternating subtidal, intertidal, and supratidal lagoonal sediments. However, dolomitization is less intense in the Condorsinga rocks compared with the Chambará and represented by isolated layers of finely crystalline dolomite near the contact with the underlying Aramachay. It has an early diagenetic origin. Bioclastic packstones at the base of the Condorsinga are in-facies with the upper Aramachay, suggesting a continuation of the unrestricted open basin setting. At Malpaso, the Condorsinga Formation is 300 m thick and consists almost exclusively of 0.3–4 m thick layers of limestone, though near the base, there are local intercalations of dolomitic limestone and calcareous dolomite. In particular, the Condorsinga has a low detrital content (<3%) and overall is horizontally laminated with bedded and nodular cherts and burrows; it contains bivalves, crinoids, and gastropods of marine affinity. Layers of gypsum occur locally near the top of the Condorsinga Formation.

The overall lagoonal succession is characterized by laminated dolomitic mudstones, bioclastic and peloidal wackestones, and packstones (Fig. 10a and b), as well as local lenses of evaporite that attest to periodic shallowing and exposure. Mold porosity, which has resulted from the dissolution of various bioclastic components, is commonly cemented by coarsely crystalline calcite. In the middle of the Condorsinga, dissolution of ooids, and subsequent

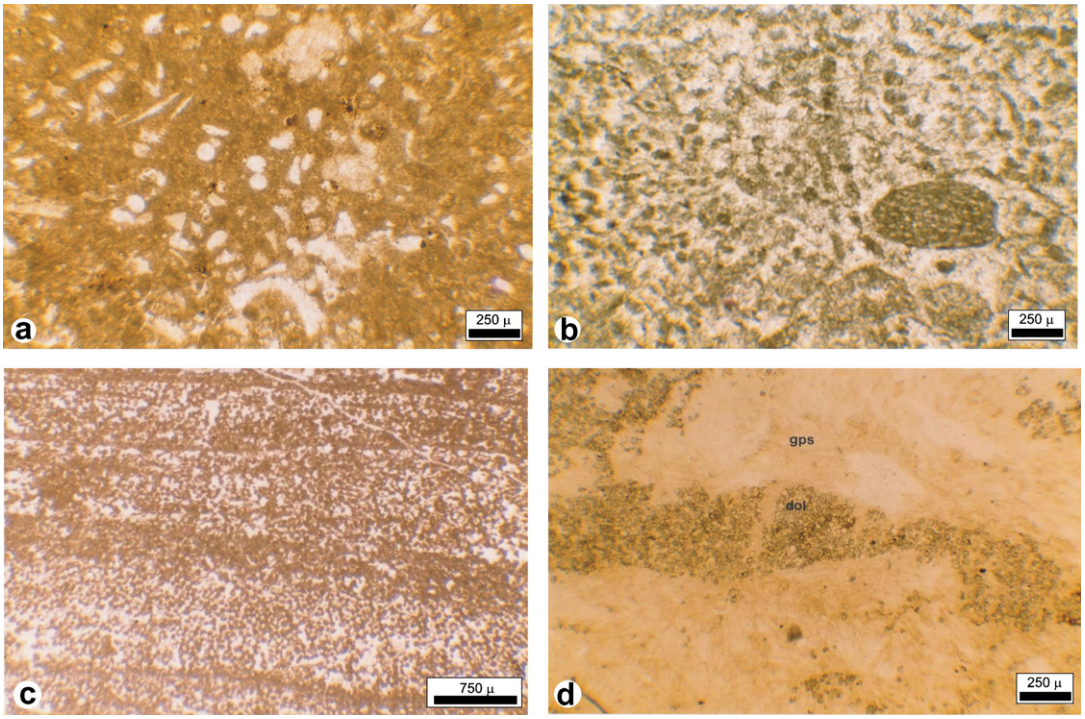

Fig. 10. Representative microscopic photographs of Condorsinga facies in the Malpaso section. (a) Peloidal and bioclastic packstone with abundant bioclasts of sponge spicules (533 m above Mitu datum). (b) Pellet grainstone with coprolites, pellets consisting of micrite and the cement of finely crystalline calcite (592 m above Mitu). (c) Intercalation of pellet pack/grainstone with algal laminae (706 m above Mitu). (d) Small planar dolomite crystals (dol) replacing gypsum (gps) along lamination (sample collected close to Malpaso section).

cementing with calcite, has occurred. The subtidal facies is characterized by oolitic and bioclastic grainstones. Chert is markedly less abundant than in the lower formations.

The intertidal and supratidal lagoonal facies consist of mudstones with algal laminations and supratidal breccias. In the upper part of the Condorsinga, algal-laminated sediments are associated with smooth algal mats. These algal-laminated sediments have low organic content and are composed of fine-grained, pelletal sands with interlaminated algal-rich layers (Fig. 10c). In the Paccha area, there are several gypsum lenses in the middle of the Condorsinga Formation. The gypsum consists of thick units of laminated gypsum interbedded with intertidal and subtidal dolomites (Fig. 10d); in some places, small idiomorphic crystals of dolomite replace gypsum along the laminations. Hypersaline conditions might explain not only the accumulations of gypsum but also other sediments containing smooth algal mats, which in modern environments are symptomatic of the outer intertidal zone in sheltered hypersaline embayments (Davies, 1970). Reflection seismic shows that, on a basin scale, hypersaline salt accumulation has been substantial enough to form diapiric structures (G. Wine, pers. commun. 2003).

4.2. Tectonostratigraphic reconstruction

The Pucará Basin formed on a platform of deformed Permo-Carboniferous and Lower Triassic rocks (Figs. 2 and 11). The Upper Carboniferous and Permian Tarma–Copacabana succession of terrigenous clastic sediments was deposited in a complex of extensional basins associated with NW- to NNW-directed shear zones (Tankard et al., 2006). Fault-controlled subsidence gradually diminished during the Late Permian and was replaced by a phase of postrift subsidence, forming a broad epeiric sea. The argillaceous, organic-rich Ene Formation was deposited as a regional blanket or drape. However, there appears to be a conspicuous lateral offset of the locus of postrift Ene subsidence compared to the preceding rift complex. Kusznir and Egan (1989) model similar basin characteristics elsewhere and attribute these characteristics to separate upper-crustal simple-shear and lower-crustal pure-shear processes. The Tarma–Copacabana–Ene succession was deformed by massive structural inversion during the latest Permian–Early Triassic Juruá (Tankard, 2001).

The Pucará evolved as a post-rift phase of basin subsidence above the previous tract of Mitu rifts (Fig. 11). Similar to its earlier counterpart, fault-controlled subsidence decreased with progressive relaxation of the extensional stresses and was replaced by widespread regional subsidence as the various rift depocenters were yoked together. The transition was gradual, so the lower Pucará in particular remained subject to substantial thickness changes (Figs. 1, 5, and 6), as well as facies variations along some still active, preexisting fault trends, as shown by the drastic thinning of the Chambará section from Malpaso to Tingocancha at the basin edge. The succession expands basin-

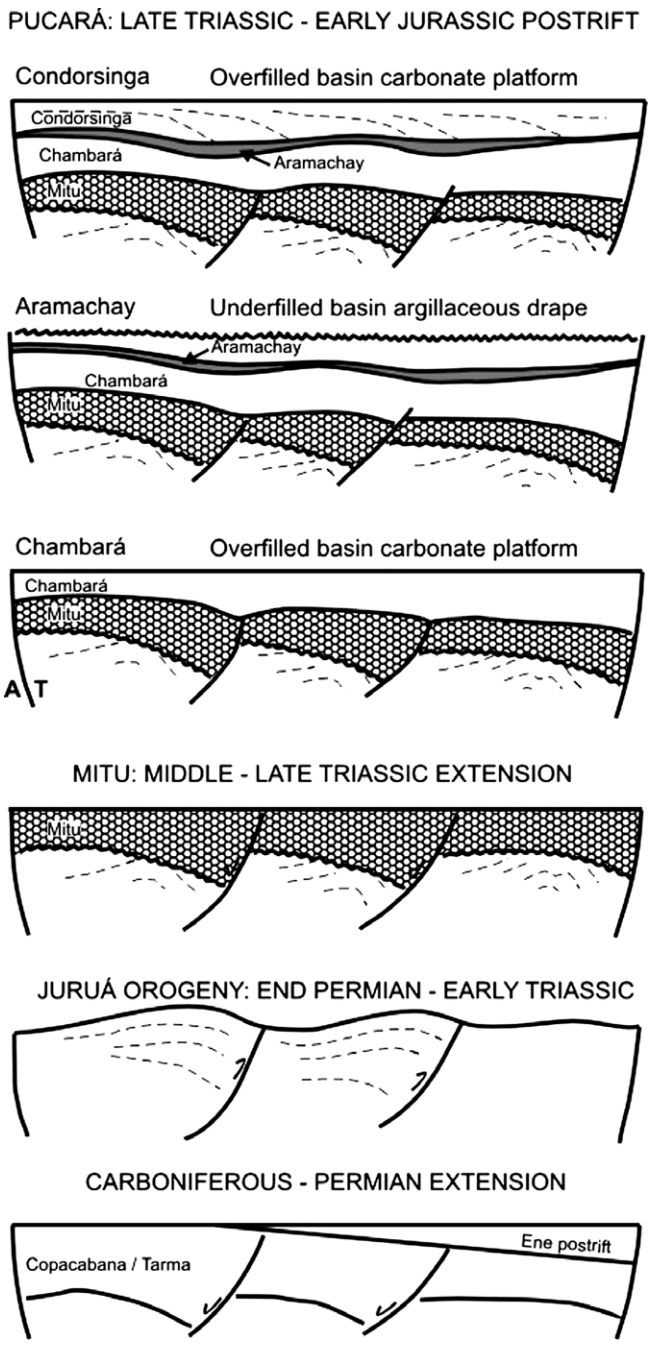

Fig. 11. Schematic summary of late Paleozoic and early Mesozoic basin evolution by persistent reworking of older basement faults (cf. Fig. 2). The Copacabana–Ene landscape of Carboniferous–Permian time involved extension and postrift subsidence; note lateral offset of the postrift prism. By the end of the Permian and during the Early Triassic, older stratigraphy was deformed in the Juruá orogeny by massive structural inversion. A new cycle of fault-controlled extension formed the Early–Middle Triassic Mitu basins through orogenic collapse. The Pucará cover developed above the Mitu landscape as earlier Mitu depocenters yoked together into a broad postrift epeiric basin. The transition from rift to postrift is marked by the Chambará Formation, with substantial thickness variations where some faulting persisted. The transitional postrift episode consisted of a carbonate platform that filled the basin to a depositional base level. During the Aramachay phase of basin overdeepening, sediment starvation and deep-water conditions are reflected in the widespread argillaceous drape. Basin overfilling marked the closing episode of the Pucará Basin with the development of the Condorsinga carbonate platform.

ward (Fig. 5). Eustatic processes were important, but we are unable to separate them from the overriding effects of tectonic subsidence that are characteristic of the plate margin.

Figs. 6 and 12 summarize the tectonostratigraphic relationships of the threefold Pucará subdivision. We interpret the Chambará carbonate platform as the transition from fault-controlled rift to regional postrift subsidence. Thickness variations are marked, especially along marginal or intrabasinal shear zones; the significant changes in thickness from San Vicente to Vilcapoma (Fig. 1a and Fig. 5) coincide with a fault splay. Nevertheless, a stacked succession of subtidal, intertidal, and supratidal facies associations built a shoal-water carbonate platform as an overfilled basin complex ($\mathrm{Rate}_{\mathrm{subsidence}} > \mathrm{Rate}_{\mathrm{deposition}}$). The Aramachay deep-water drape accumulated during a protracted phase of basin deepening and inundation, probably unassisted by significant active faulting, because the drape does not vary substantially in thickness. The ubiquitous organic-rich argillaceous limestones, shales, and mudstones indicate that the basin was underfilled ($R_s < R_d$), and that structural or topographic relief was insufficient to contribute significant diluting terrigenous clastic sediments. Gradual filling of the basin is suggested by the upward-coarsening upper parts of the Aramachay. The succeeding Condorsinga carbonate platform is locally infacies as the basin gradually filled to the depositional base level in the manner of the earlier Chambará platform ($R_s < R_d$). Together, these three units sketch the overall pattern of postrift subsidence and overdeepening marked by the sediment-starved Aramachay phase.

At Malpaso locality, the stacking of four shallowing-upward Chambará sequences and maximum flooding deposits of the basal Aramachay are similar to the transgressive parasequence sets of Van Wagoner et al. (1990), except that we envisage accumulation almost entirely by tectonic accommodation. Ammonite faunas in the Aramachay indicate flooding had normal marine salinities.

Each of the first three shallowing-upward sequences typically consists of subtidal lagoonal facies near the base, and thin ($\leqslant$3 m) intertidal to supratidal facies locally cap them. These three shallowing-upward sequences are completely present only at Malpaso (Fig. 5). The fourth shallowing-upward sequence has the characteristics of open-marine sedimentation, including well-developed crinoidal banks and interfingering lagoonal subtidal facies; at Tingocancha, they consist of intraclastic, bioclastic and peloidal wackestones–packstones, grapestones, and bioclastic to oolitic grainstones and coprolites. The relatively deeper-water Aramachay facies heralds the maximum flooding that drowned the fourth sequence. The hard-grounds in the Malpaso section mark the transition from marine basinal deposition to the deeper-water accumulations of the underfilled basin. These deep-water facies rest directly on subtidal facies at Tingocancha, suggesting that subsidence was rapid during the upper Chambará. Furthermore, the Malpaso hard-grounds indicate sedimentation rates decreased significantly, resulting in a sediment-starved basin and sedimentary hiatus.

Comparing the facies trends of Malpaso and Tingocancha, it is apparent that marine flooding was from northwest to southeast. This interpretation is supported by the presence of deeper-water facies at the top of the Chambará succession at Malpaso, whereas peritidal facies persisted at Tingocancha. On the scale of the entire Pucará basin, we know that overall inundation progressed from northwest to southeast along the axis of a fault-controlled trough (Figs. 1 and 6). Paleontological and sedimentological studies of exposures in the Utcubamba Valley of northern Peru show that the Aramachay deep-water facies are Rhaetian in age (Prinz, 1985a), whereas their counterparts in the southern part of the basin are Hettangian.

The highstand systems tract or regressive regime of the Aramachay–Condorsinga transition consists mainly of lagoonal facies at Tingocancha (bioclastic wackestones, packstones) and a more basinal carbonate platform at Malpaso (bioclastic packstones and mudstones, crinoidal

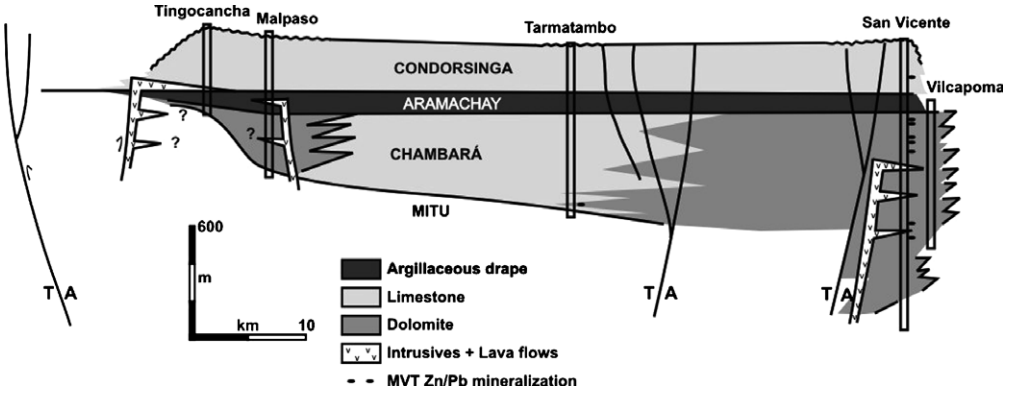

Fig. 12. Interpreted tectonostratigraphic cross-section. Shalipayco column is excluded because it is situated off section, but it samples the same strike-slip fault zone as San Vicente and Vilcapoma. The SW and NE margins are formed by left-lateral shear zones. Intrusive and extrusive magmas at the Yauli dome took advantage of dilation at a releasing bend. Magmatism and later weak metamorphism coincide with dolomitization, suggesting fault-controlled hydrothermal processes. Likewise, Cenozoic-age dolomitization and MVT lead-zinc mineralisation along the NE margin coincide with a shear zone.

banks, other marine invertebrate fauna). A hard-ground separates the lagoonal facies from the underlying deeper-water facies at Tingocancha. Furthermore, evaporites occur as pseudomorphs in the lower part of the Condorsinga at Tingocancha and lenses elsewhere, whereas at Malpaso, evaporite minerals are restricted to the top of the Condorsinga. These observations imply that the upper Pucará regression proceeded from southeast to northwest, a reversal of the axial flooding of earlier in the Pucará.

Transgressive flooding was widespread during the Hettangian. Counterparts of the relatively deep-water Aramachay facies of Peru are present in Chile (Hillebrandt, 1973; Hillebrandt et al., 1986) and Colombia (Geyer, 1979). These results match the Hettangian transgressive/regressive switch in the Exxon global sea-level chart, except that in the Exxon scheme, this Hettangian event is subordinate to other Late Triassic–Early Jurassic events (e.g., Vail et al., 1984; Haq et al., 1988). This discrepancy is not surprising because marine inundation in the Peruvian Pucará Basin was driven primarily by tectonism. We do not discredit eustatic influences but observe that we are unable to separate strictly eustatic processes from tectonic ones in such a dynamic tectonic setting. In his interpretation of a eustatic curve for the basins along the western margin of the South American cratons, Hallam (1988, 1991) assigns maximum flooding to the Sinemurian based on a misconception that the Aramachay black limestones and shales were of that age.

5. Discussion

The Pucará succession in central Peru has a threefold subdivision with distinct lithological, facies, paleontological, and geochemical characteristics. The argillaceous Aramachay sediments with deeper-water facies affinities are conspicuous in each section and provide the basis for the threefold division into the Chambará, Aramachay, and Condorsinga formations, which reflect unique episodes of basin subsidence. The Chambará and Condorsinga formations were constructed by shallow-water sedimentation, mainly carbonate platforms with lagoon-like oolitic subtidal, intertidal, and supratidal facies. Basinal facies resembling modern marine shelves (i.e., unrestricted circulation) also occur, albeit less abundantly, at various places in the Chambará succession. The depositional model envisaged is in many respects similar to the tidal lagoon and oolitic shoal environments in the modern era (cf. Shinn, 1983; Wilson and Jordan, 1983). At Malpaso, the shallow-water facies form stacked shallowing-upward sequences due to intermittent fault-controlled subsidence. The subtidal facies tracts consist typically of oolitic grainstones and subordinate bioclastic packstones. Reef buildups have not been recognized.

In our facies analysis of the Pucará succession, we repeatedly refer to lagoonal facies tracts and have interpreted them as subtidal, intertidal, and supratidal. Similar to most facies analyses, our interpretation derives from comparison with published models. In this respect, these facies resemble their counterparts in modern lagoonal and back-barrier settings, suggesting similar processes of sedimentation. However, the Late Triassic–Early Jurassic Pucará Basin was an elongate, NNW-oriented trough with fault-bounded margins (Fig. 1b and Fig. 6), whose western margin abuts a basement high described as the Divisoria Arch (Benavides, 1999). Our stratigraphic analysis shows westward thinning of the basin fill and facies variations that imply that this structural high was, if not emergent, at least able to supply reworked detritus. While it has been suggested that the basin opened to the ocean only in the northwest (Szekely and Grose, 1972; Mégard, 1978), we observe that the ammonite faunas and other marine invertebrate biota indicate normal marine salinities and that the facies characteristics of the carbonate-dominated succession recognizes no abnormal tidal ranges (unusually low or high). In this respect, we surmise that the western margin of the basin was only partially silled and allowed periodic flooding or that flooding locally used structurally controlled inlets or passes. The Pucará Basin was a 1000 km long trough, up to 300 km wide in places. Without direct access to the open ocean, tides would have been damped (e.g., as in the modern Mediterranean) and salinities far from normal (either diluted by fresh water or hypersaline). At times, parts of the basin were hypersaline, as shown by local reflection seismic evidence of massive evaporites and diapirism (G. Wine, pers. commun., 2003). Sedimentological interpretation generally relies considerably on modern analogs in reconstructing ancient landscapes, but it frequently fails to recognize the unique landscapes with no modern counterparts.

The western and eastern margins of the Chambará depocenter have higher detrital content than the more basinal parts. In the west, this situation may have resulted from erosional reworking along the fault-bound structural high (Divisoria Arch, Benavides, 1999), consistent with periodic flooding. In other words, the Pucará was a silled basin that did not rely solely on a distant entrance in the northwest to maintain its marine circulation. In contrast, the higher detrital content of the eastern margin of the basin, which consists of mixed terrigenous clastic–evaporitic facies, reflects the influence of the nearby Brazilian–Guyana shield (Fig. 1a).

The Pucará Basin foundered during the Aramachay, and the low rates of sediment influx formed an underfilled argillaceous basin. The lithologies and ammonite faunas are compatible with a relatively deep-water milieu. The vertical transition from shallow-water Chambará sedimentation to deeper-basin Aramachay facies is characterized by crinoidal banks and biomicrites that resemble modern, open marine shelf sediments, but we attribute them to widespread marine inundation of the broad Pucará trough. We encounter neither slope breccias nor turbidites, which suggests a general absence of steep gradients. Stratigraphic relationships show that the basin fill onlapped toward the southeast along the axis of the basin, but transgression

was augmented by flooding over the western structural high. The Condorsinga carbonate platform documents a return to shallow-water, Chambará-like deposition, and overfilled basin characteristics.

In the Pucará intertidal and supratidal facies, evaporite pseudomorphs are commonly associated with algal mats and extensive early diagenetic dolomitization, suggesting sedimentation was influenced by an arid climate in an environment comparable to modern sabkhas of the Persian Gulf (McKenzie, 1981; Patterson and Kinsman, 1982; Shinn, 1983). We observe evidence of hypersaline evaporitic conditions in the eastern part of the cross-basin transect (e.g., San Vicente area), where gypsum layers occur within redbeds. These San Vicente gypsum and redbeds mark the Mitu–Pucará transition and are associated with some overlying carbonates. In the northeast part of the study area, the Oxapampa 7-1 exploration well penetrates 1800 m of interbedded carbonates and evaporites.

Regionally, the Pucará Basin was structurally compartmentalized by NNW- and NE-trending basement faults that controlled the overall isopach distribution (Fig. 6). However, a secondary scale of compartmentalization appears due to coalescing depositional systems. In the Condorsinga landscape, it resulted in local hypersaline conditions in the lagoonal environments and deposition of massive gypsum lenses. Locally exposed earlier dolomites were reworked into detrital eolian dolomite accumulations (e.g., Malpaso section). The Chambará succession differs, in that evaporite minerals are rare and occur mainly as pseudomorphs disseminated throughout the intertidal and supratidal sabkha-type facies, except for more prominent gypsum layers associated with terrigenous clastics at the Mitu–Chambará transition and along the eastern margin.

Whereas we argue that the Pucará succession accumulated in a silled structural trough, the western margin of which permitted at least periodic spilling over of marine waters, Loughman and Hallam (1982) and Loughman (1984) attribute the carbonate prisms to a terrace wedge setting that faced the open ocean. They also attempt to explain the phosphorites that occur within the Aramachay succession. Most accounts follow Kazakov's (1937) model of direct precipitation of marine apatite from upwelled phosphate-rich waters, such as along the present Peruvian margin. In many parts of the world, the major locus of phosphate accumulation is an embayment or silled basin with direct access to open-ocean, phosphate-rich waters but that also has the advantage of organic-rich argillaceous sediments and anoxic bottom waters (cf. Gulbrandsen, 1969; Heckel, 1977). In this respect, the silled Aramachay trough is an ideal depository.

A basement-involved fault zone along the western margin not only facilitated subsidence during Aramachay time but also appears to have been the source of higher heat flows, probably due to Tertiary magmatism. This finding may explain lithological differences between Tingocancha–Malpaso and the rest of the basin. Along this structural margin, the Aramachay argillaceous drape is largely siliceous with an abundant chert component and subordinate calcite and is partly volcaniclastic. Illite-dominated clay minerals are the main detrital component. In contrast, the eastern Aramachay (e.g., Shalipayco, San Vicente) contains greater amounts of calcite and organic carbon, involves smaller amounts of chert and clay minerals, and has not suffered any significant metamorphism.

Szekely and Grose (1972) and Mégard (1978) recognize that the Pucará Basin subsided along the NNW-striking structural grain but also suggest that the basin fill was thickest along the central axis, from which it thinned more or less uniformly to both the east and west. Mégard (1979) and Benavides (1999) go even further, suggesting that the Pucará Basin was divided longitudinally by a central arch of Permian origin; this intervening basement high has been referred to as the Marañón Arch, supposedly caught up within the Late Cretaceous–Cenozoic eastern Cordillera. These interpretations contrast starkly with our structurally compartmentalized basin model, which is derived from a network of industry seismic data and fieldwork (Fig. 6). The seismic data show that this structural control involved reactivation of the earlier Mitu extensional faults (Fig. 3). During the Cenozoic, these basement-involved faults appear to have functioned as conduits for basinal brines that introduced Mississippi Valley-type mineralisation (Fontboté et al., 1995; Spangenberg et al., 1999; Moritz et al., 1996; Baudoux et al., 2001). The fault-bounded compartments resulted in marked variations of thickness and facies of the three units of the Pucará Group, due to variations in the rate of subsidence from compartment to compartment. In some areas, subsidence also involved an element of block rotation. Carbonate productivity and accumulation generally kept pace with these various patterns of subsidence, maintaining shallow-water conditions throughout (e.g., Grayson and Oldham, 1987).

Reflection seismic data and the distribution of earthquake epicenters show that the NW- to NNW-trending, basin-forming shear zones are very steep and indicate crustal-scale dimensions (Bernal et al., 2001, 2002). They not only participated in accommodating subsidence and accumulation of the Pucará cover but also significantly modified the lithologies by acting as conduits for basaltic and andesitic magmatism, as well as the basinal brines that are believed to have generated the MVT lead-zinc mineralization.

Audebaud et al. (1973) infer the presence of a volcanic arc along the western margin of the Pucará Basin. In our examination of the Pucará lithofacies, we find no evidence that the Pacific margin was a magmatic arc at this time, at least not until the upper Pucará. We examine the volcanic material in the central part of the basin at Lircay, Tingocancha, and Shalipayco and find intraplate rift affinities but no obvious volcanic arc signature. The conduits may have been local areas of dilation along the irregular fault planes (see Kontak et al., 1985). The volcanic rocks interbedded within the Pucará Group represent the final phase of transtensional fault activity (Rosas et al., 1997). How-

ever, convincing occurrences of arc-related volcanic rocks in northern Peru include late Liassic lava flows and volcaniclastic sediments, whereas Liassic arc volcanics are exposed in the southern coastal region. The evidence suggests the earliest arc magmatism in Peru dates to the Liassic, approximately the same time as in northern Chile, where Hillebrandt et al. (1986) date Hettangian–Sinemurian marine carbonates below the La Negra calc-alkaline basalts and basaltic andesites.

Finally, we show that the Mitu and Pucará basins developed as a rift–postrift pair (Fig. 11). With the relaxation of extensional stresses and declining fault activity, the various Mitu rift depocenters were yoked together to form the regionally subsiding Pucará trough (Fig. 6). In this respect, we attribute the Chambará phase of subsidence (Fig. 2) to the rift–postrift transition that mixed local fault-controlled subsidence with regional downwarping. However, this interpretation does not entirely negate fault activity during the younger Pucará. It is necessary to accommodate the continuing subsidence of the brittle crust with displacement of the principal basin-bounding faults, such as the shear zone that marked the western boundary and its association with later weak metamorphism and mineralisation. The distinction is between fault-driven subsidence during the extensional phase and mild, fault-accommodated subsidence during the transitional postrift episode.

The Phanerozoic geology of western South America comprises a repetitive history of basin development and structural modification (Tankard et al., 1995, 2006). The Mitu–Pucará rift–postrift basin complex developed above a deformed Copacabana–Ene stratigraphy of Permo-Carboniferous age (Figs. 2 and 11), from which it is separated by a prominent unconformity in a process reminiscent of the orogenic collapse of Dewey (1988). The Early Triassic Juruá orogeny developed through large-scale structural inversion of the preexisting basin complex, a deformed belt of 1400 km width (Barros and Carneiro, 1991). This orogeny is dated on the basis of seismic analysis and biostratigraphic well controls and marked by 255–236 Ma synkinematic emplacement of plutons along its grain (Lancelot et al., 1978; Dalmayrac et al., 1980; Gunnesch et al., 1990; Soler, 1991). Whereas we recognize the association of plutons with the Juruá orogeny, Sempere et al. (2002) attribute them to a protracted episode of crustal thinning. Transpressional systems such as Juruá are commonly associated with magmatism because of the steep pressure gradients in the shear zones (see Saint Blanquat et al., 1998). Throughout western Gondwana, the late Hercynian orogens were generally intracratonic and formed as a set of isolated or disconnected segments. Because of the dearth of direct information regarding the age of deformation, the Juruá orogeny and its well-constrained age are significant. An Early Triassic deformational event, interpreted from reflection seismic data and well controls, is also recognized in the central Congo Basin of western Gondwana (Daly et al., 1991; Cohydro, undated) and the Cape fold belt of South Africa.

A repetitive history of basin subsidence and deformation occurred throughout the Phanerozoic, marked by two milestones: the mid-Permian Ene and lowermost Jurassic Aramachay argillaceous drapes, which marked the dying phases of fault-controlled subsidence and are now important, organic-rich, petroleum source rocks. The various stages of basin evolution involved persistent reworking of basement fabrics probably inherited from Neoproterozoic tectonic events (Balkwill et al., 1995; Tankard et al., 1995). Accumulations of petroleum commonly occur in structural traps that developed above these older basement faults, which emphasizes the importance of understanding the tectonic and structural framework. This tectonic interpretation is equally pertinent to mineralisation. The basement-involved fault zone along the western margin facilitated subsidence of the Pucará and other basins and also may have been the source of higher heat flows, as evidenced by periodic magmatism and polymetallic ore accumulation (see Atlas Mineria, 2001). This pattern of basin subsidence and structural reworking provides an important control on Andean deformation. Substantial seismic evidence indicates that much of the Andean fold belt of Peru developed by basement-rooted transpressional deformation, local areas of thin-skinned thrusting (e.g., Ene, Madre de Dios) notwithstanding. Furthermore, the western, structurally bound Divisoria high was long lived, and in the Late Cretaceous–Paleogene (82–34 Ma), it was intruded by the Coastal Batholith. Neogene shearing resulted in domino-style rotation and uplift of the structural blocks that constitute this high (Tankard et al., 2006). We believe that the Pucará Basin offers important insights into the nature of basin subsidence and deformation, including the Andean episode, and partly explains the distribution of petroleum and ore mineral resources.

6. Conclusions

The Pucará Basin is a NNW-elongated trough, a postrift basin complex that formed as the earlier Mitu fault-controlled rifts yoked together. The three-part stratigraphic subdivision comprises lower and upper carbonate platforms with an intermediate phase of basin overdeepening and sediment starvation that resulted in a regional, organic-rich argillaceous drape. The Pucará Basin is bound both west and east by NNW-trending shear zones. There is no evidence that this paleo-Pacific margin was a magmatic arc, at least not until upper Pucará time when it was only weakly developed in northern Peru. On the basis of geochemical studies (e.g., absence of calc-alkaline lithologies), the intercalations of volcanic material throughout the Pucará succession have intraplate rift affinities. We attribute this intraplate magmatism not to rifting processes but to transtensional dilation along the planes of strike-slip faults.

Although the overall stratigraphic architecture reflects axial patterns of onlap and progradation, substantial evidence suggests flooding of the fringing high along the western margin was ubiquitous. The basin is approximately

1000 km long, and yet the ammonite faunas and other biota indicate normal marine salinities. The Chambará and Condorsinga formations consist mainly of shallow-water carbonate sediments interpreted as lagoon-like subtidal, intertidal, and supratidal deposits. We find no evidence of abnormal tidal ranges (i.e. high or low), which suggests tidal circulation was largely controlled by direct access to the open ocean, either through regular flooding of the basement high along the western margin or tidal passes. The distribution of sedimentary facies, indicative of reworking from the west, and the phosphorite occurrences in the Aramachay argillaceous fill argue compellingly for marine inundation along this margin.

The subtidal carbonate platform consists mainly of oolitic grainstones with subordinate bioclastic packstones. Reef buildups have not been recognized. Open basin facies are less abundant and consist principally of crinoidal packstones and bioclastic wackestones in the Chambará Formation. In the intertidal and supratidal facies, evaporite pseudomorphs are common, generally associated with algal mats and widespread early diagenetic dolomitization. Generally, the basin was overfilled during Chambará and Condorsinga times, so subsidence was balanced by carbonate production ($R_s < R_d$), and shallow environments prevailed. Conversely, the intermediate Hettangian–Sinemurian stage of basin subsidence was marked by underfilled conditions and deep water ($R_s < R_d$). The deeper-water Aramachay argillaceous drape is an important hydrocarbon source rock.

Facies interpretation of ancient basin fills generally relies on comparison with modern analogs and their apparent eustatic context. However, this approach frequently fails to recognize unique tectonic landscapes with no modern counterparts. We document the role of the crustal-scale shear zones in driving development of the Pucará Basin and, in this context, attempt to integrate the tectonic, stratigraphic, and sedimentological facets of basin formation.

Acknowledgments

This paper benefited immensely from discussions, at various stages of the work, with Rolando Bolaños, Juan Carlos Braga, Huldrych Kobe, José Martín, Rossana Martini, Jorge Merino, Robert Moritz, Les Oldham, and Gary Wine. A previous draft was reviewed by Ricardo Astini, Dave Barbeau, Víctor Benavides, Brian Darby, and Thierry Sempere, for which we are very grateful. We also are grateful for the willing cooperation of the Peruvian resource companies CENTROMIN, PeruPetro, and SIMSA. Finally, the project received financial support from the German Academic Exchange Service (DAAD) and Swiss National Science Foundation (FNRS).

References

Mineria, Atlas, 2001. Atlas Mineria en el Peru. Ministerio de Energia y Minas., 97 pp.

Audebaud, E., Capdevila, R., Dalmayrac, B., Debelmas, J., Laubacher, G., Levevre, C., Marocco, R., Martinez, C., Mattauer, M., Mégard, F., Paredes, J., Tomasi, P., 1973. Les traits géologiques essentiels des Andes Centrales (Pérou-Bolivie). Revue de Géographie Physique et Géologie Dynamique 15, 73–113.

Baldock, J.W., 1982. Geología del Ecuador. Boletín de la Explicación del Mapa Geológico de la República del Ecuador. Dirección General de Geología y Minas, Quito, Ecuador, 70 pp.

Balkwill, H.R., Rodrigue, G., Paredes, F.I., Almeida, J.P., 1995. Northern part of Oriente basin, Ecuador: reflection seismic expression of structures. In: Tankard, A., Welsink, H.J., Suárez, R. (Eds.), Petroleum Basins of South America, vol. 62. AAPG Memoir, pp. 559–571.

Barros, M.C., Carneiro, E. de P., 1991. The Triassic Juruá orogeny and the tectonosedimentary evolution of Peruvian Oriente basin, exploration implications. IV Simposio Bolivariano, Bogotá, Colombia, 44 pp.

Baudoux, V., Moritz, R., Fontboté, L., 2001, The Mississippi Valley-type Zn-Pb deposit of San Vicente, central Peru: an Andean syntectonic deposit. In: Piestrzynski, A. et al. (Eds). Mineral Deposits at the Beginning of the 21st Century, Proceedings of the 6th Biennial SGA Meeting, Krakow, Poland, 26–29 August 2001. Balkema, Rótterdam, pp. 191–195.

Benavides, V., 1962. Estratigrafía preterciaria de la región de Arequipa. Boletín de la Sociedad Geológica del Perú 38, 5–63.

Benavides, V., 1999. Orogenic evolution of the Peruvian Andes: The Andean Cycle. In: Skinner, B.J. (Ed.), Geology and Ore Deposits of the Central Andes, vol. 7. Society of Economic Geologists, Special Publication, pp. 61–107.

Bernal, I., Tavera, H., Antayhua, Y., 2001. Evaluacion de la sismicidad y distribucion de la energia sismica en Peru. Boletín de la Sociedad Geológica del Perú 92, 67–78.

Bernal, I., Tavera, H., Antayhua, Y., 2002. Zonas sismogénicas en Perú: volúmenes de deformación, gráficos polares y zonificación preliminar. Boletín de la Sociedad Geológica del Perú 93, 31–44.

Blau, J., Rosas, S., Senff, M., 1994. *Favreina peruviensis,* n. sp., ein Crustaceen-Mikrokoprolith aus dem Lias von Peru. Paläontologische Zeitung 68, 521–527.

Boily, M., Brooks, C., James, D.E., 1984. Geochemical characteristics of the late Mesozoic Andean volcanics. In: Harmon, R.S., Barreiro, B.A. (Eds.). Andean magmatism: chemical and isotopic constraints. Shiva, Cheshire, pp. 191–202.

Cánepa, C., 1990. Vanadiferous occurrences in the Pariatambo Formation and at Sincos Central Peru. In: Fontboté, L., Amstutz, G.C., Cardozo, M., Cedillo, E., Frutos, J. (Eds.), Stratabound Ore Deposits in the Andes. Springer, Berlin, pp. 595–597.

Cediel, F., Mojica, J., Macia, C., 1981. Las Formaciones Luisa, Payandé, Saldaña, sus columnas estratigráficas características. Geología Norandina 3, 11–19.

Chong, G., Hillebrandt, A. Von, 1985. El Triásico Preandino de Chile entre los 23°30′ y 26°oo′ de Lat. Sur. Actas del Cuarto Congreso Geológico Chileno 1, 162–210.

Cohydro, undated. The Central Congo basin, structure, stratigraphy and hydrocarbon potential. La Congolaise des Hydrocarbures, pamphlet 2.

Dalheimer, M., 1990. The Zn-Pb-Ag deposits Huaripampa and Carahuacra in the mining district of San Cristobal, central Peru. In: Fontboté, L., Amstutz, G.C., Cardozo, M., Cedillo, E., Frutos, J. (Eds.), Stratabound Ore Deposits in the Andes. Springer, Berlin, pp. 279–291.

Dalmayrac, B., Laubacher, G., Marocco, R., 1980. Caracteres généraux de l'évolution géologique des Andes péruviennes. Travaux et Documents de l'ORSTOM, Paris 122, 501.

Daly, M.C., Lawrence, S.R., Kimuna, D., Binga, M., 1991. Late Paleozoic deformation in central Africa: a result of distant collision? Nature 350, 605–607.

Davies, G.R., 1970. Algal-laminated sediments, Gladstone Embayment, Shark Bay, Western Australia. In: Logan, B.W., Davies, G.R., Read, J.F., CebulskiI, D.E. (Eds.), Carbonate sedimentation and environments Shark Bay Western Australia, vol. 13. American Association of Petroleum Geologists Memoir, pp. 169–205.

Dávila, D., Febres, O., Fontboté, L., Oldham, L., 1999. Exploración y Geología del Yacimiento San Vicente. Primer Volumen de Monografías de Yacimientos Minerales Peruanos. Volumen Luis Hochshild Plaut. ProExplo '99. Instituto de Ingenieros de Minas del Perú, pp. 305–328.

De la Cruz, J., 1995. Geología de los cuadrángulos de Santa Águeda, San Ignacio y Aramachay. Boletín del Instituto geológico, minero y metalúrgico, Serie A 57, 147.

Dewey, J.F., 1988. Extensional collapse of orogens. Tectonics 7, 1123–1139.

Fontboté, L., Gorzawski, H., 1990. Genesis of the Mississippi Valley-Type Zn-Pb deposit of San Vicente, central Peru: geologic and isotopic (Sr, O, C, S, Pb) evidence. Economic Geology 85, 1402–1437.

Fontboté, L., Spangenberg, J., Oldham, L., Dávila, D., Febres, O., 1995. The Mississippi Valley-Type zinc-lead mine of San Vicente, eastern Pucará basin, Peru International Field Conference on Carbonate-Hosted Lead-Zinc Deposits. Extended Abstracts, 83–86.

Geyer, O.F., 1979. Zur Paläogeographie mesozoischer Ingressionen und Transgressionen in Kolumbien. Neues Jahrbuch für Geologie und Paläontologie – Monatshefte 1979, 349–368.

Geyer, O.F., 1980. Die mesozoische Magnafazies-Abfolge in den nördlichen Anden (Peru, Ekuador, Kolumbien). Geologische Rundschau 69, 875–891.

Grayson, R.F., Oldham, L., 1987. A new structural framework for the northern British Dinantian as a basis for oil, gas, and mineral exploration. In: Miller, J., Adams, A.E., Wright, V.P. (Eds.), European Dinantian Environments. Wiley & Sons, pp. 33–59.

Guizado, J., Landa, C., 1966. Geología del cuadrángulo de Pampas. Boletín del Instituto geológico, minero y metalúrgico, Serie A 12, 75.

Gulbrandsen, R.A., 1969. Physical and chemical factors in the formation of marine apatite. Economic Geology 64, 365–382.

Gunnesch, K., Baumann, A., Gunnesch, M., 1990. Lead isotope variations across the central Peruvian Andes. Economic Geology 85, 1384–1401.

Gutscher, M.-A., Malavieille, J., Lallemand, S., Collot, J.-Y., 1999. Tectonic segmentation of the north Andean margin: impact of the Carnegie Ridge collision. Earth and Planetary Science Letters 168, 255–270.

Hallam, A., 1988. A reevaluation of Jurassic eustasy in the light of new data and the revised Exxon curve. In: Wilgus, C.K., Hastings, B.K., Posamentier, H., Van Wagoner, J., Ross, C.A., Kendall, C.G.S.C. (Eds.), Sea-level changes-An integrated approach. Soc. econ. Paleont. Mineralog. Spec. publ., pp. 261–273.

Hallam, A., 1991. Relative importance of regional tectonics and eustasy for the Mesozoic of the Andes. In: Macdonald, D.I.M. (Ed.), Sedimentation, tectonics, and eustasy. Sea-level changes at active margins, vol. 12. International Association of Sedimentologists, Special Publication, p. 518.

Haq, B.U., Hardenbol, J., Vail, P.R., 1988. Mesozoic and Cenozoic chronostratigraphy and eustatic cycles. In: Wilgus, C.K., Hastings, B.K., Posamentier, H., Van Wagoner, J., Ross, C.A., Kendall, C.G.S.C. (Eds.), Sea-level changes-An integrated approach, vol. 42. Soc. econ. Paleont. Mineralog. Spec. publ., pp. 71–108.

Harrison, J.V., 1943. Geología de los Andes centrales en parte del departamento de Junín (Perú). Boletín de la Sociedad Geológica del Perú 16, 97 pp.

Hasler, C.A., 1998. Facies characterization and sedimentary model of the carbonate host rock (Upper Triassic–lower Liassic) at the Mississippi Valley-type Zn–Pb ore deposit of San Vicente, Central Peru. Unpublished M. Sc. Thesis, University of Geneva, 57 pp.

Heckel, P.H., 1977. Origin of phosphatic black shale facies in Pennsylvanian cyclothems of mid-continent North America. American Association of Petroleum Geologists Bulletin 61, 1045–1068.

Hillebrandt, A. von, 1973. Neue Ergebnisse über den Jura in Chile und Argentinien. Münster. Forsch. Geol. Paläont. 31/32, 167–199.

Hillebrandt, A. von, Gröschke, M., Prinz, P., Wilke, H.G., 1986. Marines Mesozoikum in Nordchile zwischen 21° und 26°S. Berliner geowissenschaftlicher Abhandlungen. A 66, 169–190.

INGEMMET, 1999. Mapa geológico del Perú escala 1:1000,000. Instituto Geológico Minero y Metalúrgico.

Jacay, J., 1996. Geología del cuadrangulo de Singa. Boletín del Instituto geológico, minero y metalúrgico, Serie A 67, 215.

James, D.E., Brooks, C., Cuyubamba, A., 1975. Early evolution of the central Andean volcanic arc. Carnegie Institute Yearbook 74, 247–250.

Jenks, W.F., 1948. Geología de la Hoja de Arequipa al 200,000. Instituto Geológico del Perú, Boletín 9, 204.

Kazakov, A.V., 1937. The phosphorite facies and the genesis of phosphorites. Scient. Inst. Fertil. Insectofungic (Translation) 142, 95–113.

Kobe, H.W., 1995. Evaporitas y volcánicos, Grupo Pucará, Perú central, componentes volcánicos, evaporíticos y sedimentos metalíferos en la parte occidental de ola cuenca del Grupo Pucará, Perú central. Volumen Jubilar Alberto Benavides, Sociedad Geológica del Perú, 179–191.

Kontak, D.J., Clark, A.H., Farrar, E., Strong, D.F., 1985. The rift associated Permo-Triassic magmatism of the eastern Cordillera: a precursor of the Andean orogeny. In: Atherton, W.S., Pitcher, M.P., Cobbing, E.J., Beckinsale, R.D. (Eds.), Magmatism at a plate edge. The Peruvian Andes: Glasgow, Blackie and Son, Ltd., pp. 36–44.

Kusznir, N.J., Egan, S.S., 1989. Simple-shear and pure-shear models of extensional sedimentary basin formation: application to the Jeanne d'Arc basin, Grand Banks of Newfoundland. In: Tankard, A.J., Balkwill, H.R. (Eds.), Extensional Tectonics and Stratigraphy of the North Atlantic Margins, vol. 46. AAPG Memoir, pp. 305–322.

LAGESA-CFGS Asociación, 1997. Geología de los Cuadrángulos de Satipo y Puerto Prado Boletín del Instituto geológico, minero y metalúrgico, Serie A, 86, 250.

Lancelot, J.R., Laubacher, G., Marocco, R., Renaud, U., 1978. U/Pb radiogeochronology of two granitic plutons from the eastern Cordillera (Perú) – extent of Permian magmatic activity and consequences. Geologische Rundschau 67, 236–243.

Larson, C.B., Welker, K.K., 1947. Vanadium resources of Peru. U.S Bureau of Mines, Min Trade Notes, Spec Suppl., 16.

Loughman, D.L., 1984. Phosphate authigenesis in the Aramachay Formation (Lower Jurassic) of Peru. Journal of Sedimentary Petrology 54, 1147–1156.

Loughman, D.L., Hallam, A., 1982. A facies analysis of the Pucará Group (Norian to Toarcian carbonates, organic-rich shale and phosphate) of central and northern Peru. Sedimentary Geology 32, 161–194.

Mathalone, J.M.P., Montoya, M., 1995. Petroleum geology of the sub-Andean basins of Peru. In: Tankard, A.J., Suárez Soruco, R., Welsink, H.J. (Eds.), Petroleum Basins of South America, vol. 62. AAPG memoir, pp. 423–444.

McKenzie, J.A., 1981. Holocene dolomitization of calcium carbonate sediments from the coastal sabkhas of Abu Dhabi, UAE: a stable isotope study. Journal of Geology 89, 185–198.

McLaughlin, D.H., 1924. Geology and physiography of the Peruvian cordillera, departments of Junin and Lima. Geological Society of America Bulletin 35, 591–632.

Mégard, F., 1968. Geología del cuadrángulo de Huancayo. Boletín del Servicio de geología y minería 18, 123 p.

Mégard, F., 1978. Etude géologique des Andes du Pérou central. Mem. ORSTOM, Paris, 86, 310 p.

Mégard, F., 1979. Estudio geológico de los Andes del Perú central. Boletín del Instituto Geológico, Minero y Metalúrgico, 8, serie D, 227.

Mégard, F., Marocco, R., Vicente, J., Muñoz, C., Pastor, R., Mégard-Galli, J., 1983. Apuntes sobre la geología de Lircay (Huancavelica, Perú Central), el plegamiento tardihercínico y las modalidades del plegamiento andino (fase Quechua). Boletín de la Sociedad Geológica del Perú 71, 255–262.

Morche, W., Larico, W., 1996. Geología del Cuadrángulo de Huancavelica. Instituto Geológico Minero y Metalúrgico, Boletín, Serie A 73, 172 pp.

Moritz, R., Fontboté, L., Spangenberg, J., Rosas, S., Sharp, Z., Fontignie, D., 1996. Sr, C, and O isotope systematics in the Pucará basin, central Peru: comparison between Mississippi Valley-Type deposits and barren areas. Mineralium Deposita 31, 147–162.

Muñoz, C., Farfán, C., López, G., Rosas, S., 2000. Vulcanismo asociado a los carbonatos del Grupo Pucará (Triásico superior – Liásico) en el área de Shalipayco, Junín – Perú central. Resúmenes X Congreso Peruano de Geología. Sociedad Geológica del Perú, Publicación Especial 2, 42.

Palacios, O., 1980. El grupo Pucará en la región Subandina (Perú central). Boletín de la Sociedad Geológica del Perú 67, 153–162.

Pardo, A., Sanz, V., 1979. Estratigrafía del curso medio del Río La Leche, Departamento de Lambayeque. Boletín de la Sociedad Geológica del Perú 60, 251–266.

Paredes, J., 1994. Geología del Cuadrángulo de Jauja. Boletín del Instituto Geológico, Minero y Metalúrgico, Serie A. 48, 104 p.

PARSEP, 2002. Informes sobre las cuencas hidrocarburiferas peruanas. PeruPetro Promotional CD.

Patterson, R.J., Kinsman, D.J.J., 1982. Formation of diagenetic dolomite in coastal sabkhas along the Arabian (Persian) Gulf. American Association of Petroleum Geologists Bulletin 66, 28–43.

Pilger, R., 1981. Plate reconstructions, aseismic ridges, and low-angle subduction beneath the Andes. Geological Society of America Bulletin 92, 448–456.

Pilger, R., 1983. Kinematics of the South American subduction zone from global plate reconstructions. Geodynamic Series 9, 113–125.

Prinz, P., 1985a. Stratigraphie und Ammonitenfauna der Pucará-Gruppe (Obertrias-Unterjura) von Nord-Peru. Palaeontographica Abt. A 188, 153–197.

Prinz, P., 1985b. Zur Stratigraphie und Ammonitenfauna der Pucará-Gruppe bei San Vicente (Depto. Junín, Peru). Newsl. Stratigr. 14, 129–141.

Rangel, Z., 1978. Fósiles de Lircay-Uruto. Boletín del Instituto Geológico, Minero y Metalúrgico, Serie D 6, 35 p.

Reyes, L., Caldas, J., 1987. Geología de los cuadrángulos de Las Playas, La Tina, Las Lomas, Ayabaca, San Antonio, Chulucanas, Morropón, Hunacabamba, Olmos y Pomahuaca. Boletín del Instituto geológico, minero y metalúrgico, Serie A 39, 84 pp.

Romeuf, N., 1994. Volcanisme Jurassique et metamorphisme en Equateur et au Perou. Ph.D. Thesis Universite de Marseille. Faculte des Sciences et Techniques de St-Jerome, 305 p.

Romeuf, N., Aguirre, L., Soler, P., Féraud, G., Jaillard, E., Ruffet, G., 1995. Middle Jurassic volcanism in the northern and central Andes. Revista Geológica de Chile. 22, 245–259.

Rosas, S., 1994. Facies, diagenetic evolution, and sequence analysis along a SW-NE profile in the southern Pucará basin (Upper Triassic–Lower Jurassic), central Peru. Heidelberger Geowissenschaftliche Abhandlungen 80, 337 p.

Rosas, S., Fontboté, L., 1995. Evolución sedimentológica del Grupo Pucará (Triásico superior – Jurásico inferior) en un perfil SW-NE en el centro del Perú. Volumen Jubilar Alberto Benavides, Sociedad Geológica del Perú, 279–309.

Rosas, S., Fontboté, L., Morche, W., 1996. Within-plate volcanism in Upper Triassic to Lower Jurassic Pucará Group carbonates (central Peru) Abstracts. Third International Symposium on Andean Geodynamics, Ed. ORSTOM, Paris, p. 641–644.

Rosas, S., Fontboté, L., orche, W., 1997. Vulcanismo de tipo intraplaca en los carbonatos del Grupo Pucará (Triásico superior, Perú central) y su relación con el vulcanismo del Grupo Mitu (Pérmico superior – Triásico). IX Congreso Peruano de Geología. Resúmenes Extendidos, Sociedad Geológica del Perú, Vol. Esp. 1, pp. 393–396.

S & Z Consultores, 1997. Geología de los cuadrángulos de Bajo Pichanaqui y Puerto Bermúdez. Boletín del Instituto geológico, minero y metalúrgico, Serie A, 85, 180.

Sánchez, A., 1995. Geología de los cuadrangulos de Bagua Grande, Jumbilla, Lonya Grande, Chachapoyas, Rioja, Leimebamba y Bolívar. Boletín del Instituto geológico, minero y metalúrgico, Serie A 56, 400 pp.

Saint Blanquat, M., Tikoff, B., Teyssier, C., Vigneresse, J.L., 1998. Transpressional kinematics and magmatic arcs. In: Holdsworth, R.E., Strachan, R.A., Dewey, J.F. (Eds.), Continental Transpressional and Transtensional Tectonics, vol. 135. Geological Society, Special Publication, London, pp. 327–340.

Sempere, T., Carlier, G., Carlotto, V., Jacay, J., 1998. Rifting Pérmico superior – Jurásico medio en la Cordillera Oriental de Perú y Bolivia. XIII Congreso Geológico Boliviano, Potosí, Memorias 1, 31–38.

Sempere, T., Carlier, G., Carlotto, V., Jacay, J., Jiménez, N., Rosas, S., Soler, P., Cárdenas, J., Boudesseul, N., 1999. Late Permian-early Mesozoic rifts in Peru and Bolivia, and their bearing on Andean-age tectonics. IV International Symposium on Andean Geodynamics, Göttingen, Abstracts, pp. 680–685.

Sempere, T., Carlier, G., Soler, P., Fornari, M., Carlotto, V., Jacay, J., Arispe, O., Néraudeau, Cárdenas, J., Rosas, S., Jiménez, N., 2002. Late Permian – Middle Jurassic lithospheric thinning in Peru and Bolivia, and its bearing on Andean-age tectonics. Tectonophysics 345, 153–181.

Senowbari-Daryan, B., Stanley, G.D., 1986. Thalassinid anomuran microcoprolites from Upper Triassic carbonate rocks of central Peru. Lethaia 19, 343–354.

Shinn, E.A., 1983. Tidal flat environment. In: Scholle, P.A., Bebout, D.G., Moore, C.H. (Eds.), Carbonate Depositional Environments, vol. 33. American Association of Petroleum Geologists Memoir, pp. 172–210.

Soler, P., 1991. Contribution à l'étude du magmatisme associé aux zones de subduction. Pétrographie, géochimie isotopique des roches intrusives sur un transect des Pérou central. Implications géodynamiques et métallogéniques. Thèse de doctorat d'Etat, Université Pierre-et-Marie-Curie (Paris VI). 950 pp.

Spangenberg, J., Fontboté, L., Macko, S.A., 1999. Trace element and sulfur isotope geochemistry of the San Vicente Mississippi Valley-type zinc-lead district, central Peru: implications for ore fluid composition, mixing processes and sulfate reduction. Economic Geology 94, 1067–1092.

Stanley, G.D. (Ed.), 1994. Paleontology and stratigraphy of Triassic to Jurassic rocks in the Peruvian Andes. Palaeontographica Abt. A, 233, 208 p.

Szekely, T.S., Grose, L.T., 1972. Stratigraphy of the carbonate, black shale, and phosphate of the Pucará Group (Upper Triassic-Lower Jurassic), central Andes, Peru. Geological Society of America Bulletin 83, 407–428.

Tankard, A., Uliana, M.A., Welsink, H.J., et al., 1995. Structural and tectonic controls of basin evolution in southwestern Gondwana during the Phanerozoic. In: Tankard, A., Suárez, R., Welsink, H.J. (Eds.), Petroleum Basins of South America, vol. 62. American Association of Petroleum Geologists Memoir, pp. 5–52.

Tankard, A., 2001. Tectonic framework of basin evolution in Peru. Proprietary Report.

Tankard, A., Welsink, H.J., Aukes, P., 2006. Basin development along the Pacific margin of South America. A petroleum exploration perspective. In Backbone of the Americas, Joint GSA-AGA meeting, Mendoza, 3–7 April 2006. Abstracts with Program. p. 83.

Vail, P.R., Hardenbol, J., Todd, R.G., 1984. Jurassic unconformities, chronostratigraphy, and sea-level changes from seismic stratigraphy and biostratigraphy. In: Schlee, J.S. (Ed.), Interregional Unconformities and Hydrocarbon Accumulation, vol. 36. American Association of Petroleum Geologists Memoir, pp. 129–144.

Van Wagoner, J.C., Mitchum, R.M., Campion, K.M., Rahmanian, V.D., 1990. Siliciclastic sequence stratigraphy in well logs, cores, and outcrops. American Association of Petroleum Geologist Methods in Exploration Series 7, 55 pp.

Vicente, J.C., 1981. Elementos de la estratigrafía mesozoica sur-peruana. In: Volkheimer, W. and Musacchio, E. (Eds.). Cuencas sedimentarias del Jurásico y Cretácico de América del Sur, 1, pp. 319–351.

Vicente, J.C., Beaudoin, B., Chávez, A., Leon, I., 1982. La cuenca de Arequipa (Sur Peru) durante el Jurásico-Cretácico inferior. 5° Congr. Latinoam. Geol, Argentina, ACTAS 1, 121–153.

Weaver, Ch.E., 1942. A general summary of the Mesozoic of South America. In: Proc. 8th Amer. Sci. Congr., 4 (Geol. Sci.), 14.

Wilson, J.L., Jordan, C., 1983. Middle shelf environment. In: Scholle, P.A., Bebout, D.G., Moore, C.H. (Eds.), Carbonate Depositional Environments, vol. 33. American Association of Petroleum Geologists Memoir, pp. 297–343.